Theses and Dissertations | 1. Thesis and Dissertation Collection, all items

2009-12

High resolution spectrum estimation for digital tracking array

Yeo, Kwang Hui

Monterey, California: Naval Postgraduate School

http://hdl.handle.net/10945/4319

NAVAL POSTGRADUATE SCHOOL

MONTEREY, CALIFORNIA

THESIS

HIGH RESOLUTION SPECTRUM ESTIMATION FOR DIGITAL TRACKING ARRAY

by

Kwang Hui Yeo

December 2009

Thesis Advisor: David C. Jenn
Second Reader: Phillip E. Pace

THIS PAGE INTENTIONALLY LEFT BLANK

1. AGENCY USE ONLY *(Leave blank)*	2. REPORT DATE December 2009	3. REPORT TYPE AND DATES COVERED Master's Thesis
4. TITLE AND SUBTITLE High Resolution Spectrum Estimation for Digital Tracking Array		5. FUNDING NUMBERS
6. AUTHOR(S) Kwang Hui Yeo		
7. PERFORMING ORGANIZATION NAME(S) AND ADDRESS(ES) Naval Postgraduate School Monterey, CA 93943-5000		8. PERFORMING ORGANIZATION REPORT NUMBER
9. SPONSORING /MONITORING AGENCY NAME(S) AND ADDRESS(ES) N/A		10. SPONSORING/MONITORING AGENCY REPORT NUMBER
11. SUPPLEMENTARY NOTES The views expressed in this thesis are those of the author and do not reflect the official policy or position of the Department of Defense or the U.S. Government.		
12a. DISTRIBUTION / AVAILABILITY STATEMENT Approved for public release; distribution is unlimited		12b. DISTRIBUTION CODE

13. ABSTRACT (maximum 200 words)

To design a high resolution spectrum estimation module as part of a digital tracking array system, the theory and mathematical formulations of several high resolution spectrum estimation methods are presented. In the implementation of a spectrum estimation system, the received signal is first down-converted to baseband frequency using single channel or in-phase (*I*) and quad-phase (*Q*) channel down-converter before it is digitized using an analog-to-digital (ADC) converter. Three distinct frequency estimation methods, namely multiple signal classification (MUSIC), estimation of signal parameters via rotational invariance techniques (ESPRIT), and multi-resolution spectrum sensing (MRSS), are simulated to detect the inherent frequencies of a test signal. The performances, such as estimation accuracy, frequency resolution, processing speed, observation time, and resilience to noise, are measured and evaluated. Comparing the simulation results, the MRSS out-performs the MUSIC and ESPRIT in terms of spectral resolution, estimation accuracy, and robustness to noise. Though the MRSS requires a higher observation time and processing time, the values remain significantly low at 13 μs and 2.4 μs, respectively, for SNR equals to -10 dB. Hence, the MRSS is proposed as the frequency estimation algorithm in the digital tracking array to provide accurate, robust, and high resolution spectrum estimation.

14. SUBJECT TERMS Spectrum Estimation, Frequency Estimation, Frequency Down-Conversion, MUSIC, ESPRIT, MRSS			15. NUMBER OF PAGES 111
			16. PRICE CODE
17. SECURITY CLASSIFICATION OF REPORT Unclassified	18. SECURITY CLASSIFICATION OF THIS PAGE Unclassified	19. SECURITY CLASSIFICATION OF ABSTRACT Unclassified	20. LIMITATION OF ABSTRACT UU

THIS PAGE INTENTIONALLY LEFT BLANK

HIGH RESOLUTION SPECTRUM ESTIMATION FOR DIGITAL TRACKING ARRAY

Kwang Hui Yeo
Major, Singapore Army
B.Eng., National University of Singapore, 2000

Submitted in partial fulfillment of the
requirements for the degree of

MASTER OF SCIENCE IN ELECTRICAL ENGINEERING

from the

**NAVAL POSTGRADUATE SCHOOL
December 2009**

Author: Kwang Hui Yeo

Approved by: David C. Jenn
       Thesis Advisor

       Phillip E. Pace
       Second Reader

       Jeffrey B. Knorr
       Professor and Chairman, Department of Electrical and Computer
       Engineering

THIS PAGE INTENTIONALLY LEFT BLANK

ABSTRACT

To design a high resolution spectrum estimation module as part of a digital tracking array system, the theory and mathematical formulations of several high resolution spectrum estimation methods are presented. In the implementation of a spectrum estimation system, the received signal is first down-converted to baseband frequency using single channel or in-phase (I) and quad-phase (Q) channel down-converter before it is digitized using an analog-to-digital (ADC) converter. Three distinct frequency estimation methods, namely multiple signal classification (MUSIC), estimation of signal parameters via rotational invariance techniques (ESPRIT), and multi-resolution spectrum sensing (MRSS), are simulated to detect the inherent frequencies of a test signal. The performances, such as estimation accuracy, frequency resolution, processing speed, observation time, and resilience to noise, are measured and evaluated. Comparing the simulation results, the MRSS out-performs the MUSIC and ESPRIT in terms of spectral resolution, estimation accuracy, and robustness to noise. Though the MRSS requires a higher observation time and processing time, the values remain significantly low at 13 μs and 2.4 μs, respectively, for SNR equals to -10 dB. Hence, the MRSS is proposed as the frequency estimation algorithm in the digital tracking array to provide accurate, robust, and high resolution spectrum estimation.

THIS PAGE INTENTIONALLY LEFT BLANK

TABLE OF CONTENTS

LIST OF FIGURES

LIST OF TABLES

THIS PAGE INTENTIONALLY LEFT BLANK

LIST OF ACRONYMS AND ABBREVIATIONS

ADC	analog-to-digital converter
AR	autoregressive
AWGN	additive white Gaussian noise
COMINT	communications intelligence
CR	cognitive radio
DF	direction finding
DFT	discrete Fourier transform
ELINT	electronic intelligence
ESPRIT	estimation of signal parameters via rotational invariance techniques
EW	electronic warfare
FFT	fast Fourier transform
FIR	finite impulse response
I	in-phase
LO	local oscillator
MRSS	multi-resolution spectrum sensing
MUSIC	multiple signal classification
PLL	phase lock loop
Q	quad-phase
RSNS	robust symmetrical number system
SIGINT	signals intelligence
SNR	signal-to-noise ratio
UAV	unmanned aerial vehicle

THIS PAGE INTENTIONALLY LEFT BLANK

EXECUTIVE SUMMARY

To design a high resolution spectrum estimation module as part of a digital tracking array system, the theory and mathematical formulations of the high resolution spectrum estimation methods, namely autoregressive (AR), multiple signal classification (MUSIC), estimation of signal parameters via rotational invariance techniques (ESPRIT), minimum norm, and multi-resolution spectrum sensing (MRSS), are presented. The basic performances and limitations are demonstrated.

In the implementation of a spectrum estimation system, the received signal is first down-converted to baseband frequency. Both the single channel and I and Q channel frequency down-converter are demonstrated. The baseband signal is digitized with an analog-to-digital (ADC) converter to provide a real or complex sampled data sequence. Three distinct frequency estimation methods, namely MUSIC, ESPRIT and MRSS, are simulated to detect the inherent frequencies of a test signal. The performances of the three methods based on estimation accuracy, frequency resolution, processing speed, observation time, and resilience to noise, are measured and evaluated.

Comparing the simulation results, the MRSS out-performs the MUSIC and ESPRIT in terms of spectral resolution, estimation accuracy, and robustness to noise. Though the MRSS requires a higher observation time and processing time, the values remain significantly low at 13 μs and 2.4 μs, respectively, for SNR equals to -10 dB. These values meet the requirements of a digital tracking array system. Hence, the MRSS is proposed as the frequency estimation algorithm in the digital tracking array to provide accurate, robust, and high resolution spectrum estimation.

THIS PAGE INTENTIONALLY LEFT BLANK

ACKNOWLEDGMENTS

I am deeply grateful to Professor Jenn for imparting valuable knowledge to me and guiding me through my research. During our thesis consultation sessions, he always listened patiently to my findings and directed me onto the correct research path. I have really appreciated his kind words of encouragement and his technical insights. His kindness has spurred me on to complete my research.

I would also like to express gratitude to my wife, Sai Yeng, for always standing by me and providing me with the comfort of home. I must also thank my daughter, Wen Xuan, for providing me with great joy in my life.

Additionally, I would like to thank my father, Yeo Hak Heng, my mother, Ang Ah Gek, and my sister, Yeo Hui Kheng, for supporting me in many important decisions throughout my life.

Finally, I would like to thank the Singapore Armed Forces for giving me this opportunity for professional development, and the experience of studying in the United States.

THIS PAGE INTENTIONALLY LEFT BLANK

I. INTRODUCTION

A. NEED FOR FREQUENCY ESTIMATION

In a typical wireless radio communication scenario, a radio transmitter modulates its baseband frequency signal with a pre-determined high frequency carrier before transmitting the combined signal into free space. To retrieve the baseband signal, a receiver has to tune to the same carrier frequency in order to demodulate the received high frequency signal back to its baseband frequency.

As a function of electronic warfare (EW), signals intelligence (SIGINT) is the gathering of intelligence by intercepting electromagnetic signals that are transmitted into free space. The signals can be communications signals transmitted by wireless radios (communications intelligence (COMINT)), or non-communications signals transmitted intentionally or unintentionally by electronic equipment, e.g., fix all radar (electronic intelligence (ELINT)). For COMINT, the carrier frequency of an enemy's transmission is not known. The frequency has to be estimated from the received signal in a very short time, so that the signal that is received subsequently can be converted to baseband for further processing (e.g. decryption) and intelligence gathering. As the desired signal may be received along with other transmitted signals in the propagation channel, high resolution spectrum estimation is required to identify all the frequencies of the different signals, so that the frequency of the desired signal can be identified and unwanted signals can be filtered away. For ELINT, the power spectrum, including bandwidth, power, and frequency, of the received signal may reveal the identity of its transmitter.

In the operation of an unmanned aerial vehicle (UAV), the ground operator of the UAV has to maintain a continuous data link with the UAV, so as to control the UAV's flight and onboard equipment. The UAV is used to carry out a variety of military and civilian missions, such as surveillance and reconnaissance, target recognition, battle damage assessment, EW, search and rescue, and traffic monitoring [4]. A multifunction

digital tracking array system can be used to track a UAV in flight, so as to maintain a continuous data link with the UAV. In addition, it can perform other functions for COMINT and ELINT.

A possible block diagram of a tracking array system is shown in Figure 1. The order of the functions is variable, and not all functions are performed in every case. For example, when tracking and communicating with a cooperative UAV, the frequency is likely to be known so frequency estimation is not required. However, to determine the presence of emitters in the frequency band, spectral estimation must be done. Subsequent to that, direction finding (DF) as identification can be performed for COMINT. The frequency estimate would provide the initial tuning for the local oscillator (LO) and phase lock loop (PLL) to synchronize to the desired frequency. Due to the digital nature of the antenna, multiple functions can be performed on the same data.

The frequency estimation module can be designed to change and track the transmission frequency of the UAV when the latter changes frequency to enhance COMINT. Similarly, the frequency estimation module can be designed to obtain and track the transmission frequencies of several friendly UAVs.
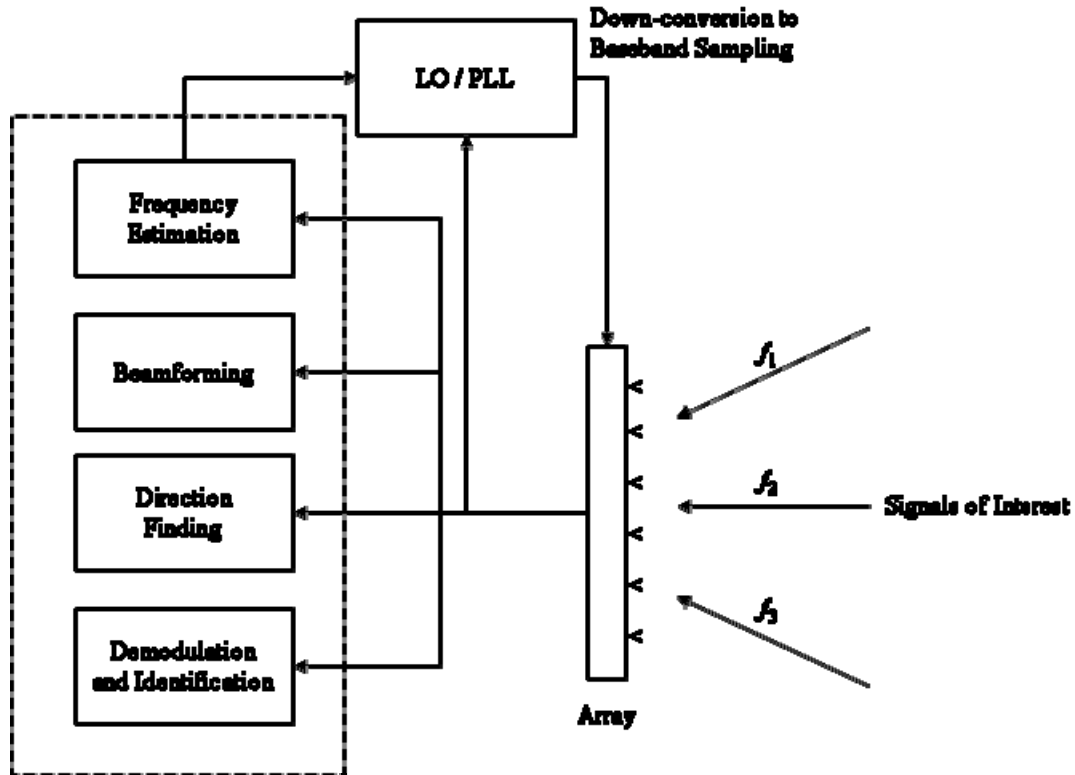
Figure 1.   Functional Block Diagram of a Multifunction Digital Tracking Array System.

B.   OBJECTIVE

The objective of this thesis is to design a high resolution spectrum estimation module as part of a multifunction digital tracking array system. Several spectrum estimation methods are analyzed and evaluated based on criteria such as estimation accuracy, frequency resolution, processing speed, observation time, and resilience to noise.

C.   PREVIOUS WORK

Gezer [1] designed and built a ground array to angle-track a UAV, so that the antenna beam of the array continues to point to the UAV in flight. This is to allow the UAV in flight to transfer data to the ground station. It was assumed that the frequency of the received signal is known.

Lee [2] designed and built a direction finding system using the robust symmetrical number system (RSNS). Due to the limitation of the sampling rate of the analog-to-digital converter (ADC), the architecture uses the in-phase (*I*) and quad-phase (*Q*) channel demodulators to down-convert the received analog signal to its baseband frequency before digitizing it. The frequency of the received signal is assumed to be known.

Kwai [3] improved on Lee's hardware to design and analyze a three-channel RSNS virtual spacing direction finding (DF) system. The frequency of the received signal is assumed to be known, and it is used to down-convert the received analog signal to its baseband frequency before digitizing it.

D.   THESIS FOCUS

This thesis focuses on the analysis and evaluation of several high resolution spectrum estimation methods, and proposes a method for integration into a digital array. In the implementation of a spectrum estimation system, the received signal is down-converted to baseband frequency. Both the single channel and *I* and *Q* channel frequency converter will be discussed. In a digital system, before frequency estimation can be performed, the signal is passed into an ADC converter to generate digital representation of the received signal in the baseband frequency. Three distinct frequency estimation methods are simulated to detect the inherent frequencies of a test signal, and their performances are measured and evaluated. Based on the simulation results, a high resolution spectrum estimation method will be proposed for the digital tracking array

E.   THESIS OUTLINE

Chapter II reviews the theory and mathematical formulations of the high-resolution spectrum estimation methods, namely autoregressive (AR), multiple signal classification (MUSIC), estimation of signal parameters via rotational invariance techniques (ESPRIT), minimum norm, and multi-resolution spectrum sensing (MRSS).

Chapter III demonstrates the implementation of a frequency estimation system with a frequency down-conversion circuit. Single channel and *I* and *Q* channel frequency conversion are presented.

Chapter IV presents the simulation results of three distinct spectrum estimation methods, namely MUSIC, ESPRIT and MRSS. Their performances in terms of estimation accuracy, frequency resolution, processing speed, observation time, and resilience to noise are measured and evaluated.

Chapter V summarizes the research findings and concludes the thesis with a recommended high-resolution spectrum estimation method for a digital tracking array.

THIS PAGE INTENTIONALLY LEFT BLANK

II. HIGH RESOLUTION SPECTRUM ESTIMATION METHODS

The first section of this chapter states the different high resolution spectrum estimation methods. In Section B, a signal is defined in the baseband frequency to demonstrate the performance of the various methods. In Section C, the evolution of Fourier transform to Fast Fourier Transform (FFT) for implementation in digital receivers is discussed. In Section D, the advantages of zero padding in FFT are presented. In Section E to Section I, the theory of the various spectrum estimation methods are reviewed and are used to generate the respective power spectrums of the baseband signal defined in Section B. The basic performances and limitations of the methods are highlighted.

A. INTRODUCTION

The Fast Fourier transform (FFT) is used in digital receivers to transform a signal between its time domain and its frequency domain representations. It is often used to generate the power spectrum of a given input signal. However, if the signal comprises two signals of very close frequencies, an FFT operation may not be able to distinguish the two frequencies [4]. Instead, only a single peak representing the two frequencies may be generated in the power spectrum. High-resolution spectrum estimation methods provide higher frequency resolution than the FFT, and they may distinguish two signals of very close frequencies with separate sharp peaks. However, high-resolution spectrum estimation techniques involve more complex operations, thus resulting in higher processing time and delay. In this chapter, the theory behind five high-resolution methods are reviewed and demonstrated. The five methods are:

1. Linear predication or autoregressive (AR)
2. Multiple signal classification (MUSIC)
3. Estimation of signal parameters via rotational invariance techniques (ESPRIT)
4. Minimum norm
5. Multi-resolution spectrum sensing (MRSS)

Prior to spectrum estimation, additional processing may be required to determine the total number of frequencies within the frequency band of interest. Other inputs such as the order of the filter may be required. After a power spectrum is generated, additional processing is required to identify the frequencies in the signal that are represented by the peaks.

B.   INPUT TEST SIGNAL

To better illustrate the operations and performances of the different spectrum estimation methods, a noiseless test signal in the baseband is generated and simulated with the different methods. The signal consists of three signals of different amplitudes, phases, and frequencies, namely 21 MHz, 36 MHz, and 38 MHz. It is represented by the equation

$$x(n) = \cos(2\pi \cdot 21 \times 10^6 \cdot n + 0.1) + 2\cos(2\pi \cdot 36 \times 10^6 \cdot n) + 1.9\cos(2\pi \cdot 38 \times 10^6 \cdot n) \quad (1)$$

where $n = 0,1,...,$ 31. The test signal is sampled 32 times at 100 MHz to create a data sequence of length 32. That is, the signal is captured over a period of 0.32 μs. A medium-range ADC can support up to 100 MHz of sampling rate. It is noted that two of the frequencies are relatively close to each other. According to Nyquist sampling theorem, since the sampling rate of 100 MHz is greater than twice the highest frequency component at 38 MHz, the analog test signal can be represented and reconstructed from the sampled data sequence, without any data lost.

C.   FAST FOURIER TRANSFORM (FFT)

The Fourier transform is based on the concept that any function in the time domain can be represented by an infinite number of sinusoidal functions [4]. The Fourier transform of a function $x(t)$ in the time domain t is given by $X(f)$ in the frequency domain f as follows:

$$F[x(t)] \equiv X(f) = \int_{-\infty}^{\infty} x(t)e^{-j2\pi ft} dt \qquad (2)$$

However, $x(t)$ must be represented in closed form so that the Fourier integral can be evaluated.

The Discrete Fourier Transform (DFT) is used to implement the Fourier transform in digital receiver. Unlike the Fourier transform, the DFT can be applied to any kind of digitized input data [4]. It is noted that the DFT only provides an approximate solution to that of the Fourier transform, especially for data sequence of short length. The DFT of $x(t)$ is performed in discrete time for $n = 0, 1,\ldots, N$ -1 as follows:

$$X(k) = \sum_{n=0}^{N-1} x(n)e^{\frac{-j2\pi kn}{N}} \qquad (3)$$

However, the DFT is generally computational intensive, and it requires N^2 computational operations to calculate the complete DFT of N frequency points.

Based on the symmetry of $e^{-j2\pi nk}$, the Fast Fourier Transform (FFT) was derived as an efficient way to calculate the DFT. The FFT and DFT produce the same characteristics and properties. The computations can be reduced from N^2 operations to $(N/2)\log_2(N)$ operations. However, the number of data points must be a power of 2 in order to take advantage of the fast computation.

The FFT of the test signal from Eq. (1) is shown in Figure 2. The power spectrum displays a sharp peak at 21 MHz and a broader peak that spans from 36 MHz to 38 MHz. Thus, the frequencies 36 MHz and 38 MHz cannot be distinguished from the spectrum using the FFT using an observation time of 0.32 μs.
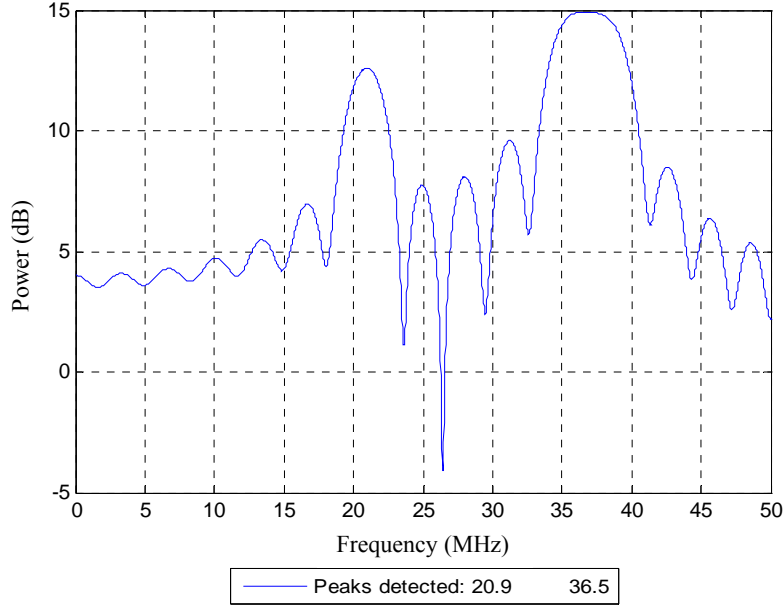
Figure 2.   Power Spectrum of Test Signal Using FFT.

D.   ZERO PADDING TO SAMPLED DATA SEQUENCE

Zero padding is the appending of zeros at the end of a sampled data sequence before the FFT is performed. It makes the locations of the peaks and sidelobes of a power spectrum more distinguishable, and enhances the accuracy of identifying the frequencies at the peaks [4]. However, this does not mean that the spectral resolution is increased [5]. The widths of the peaks remain the same with zero padding, and closely-spaced frequencies will remain undifferentiated. To increase the spectral resolution, the length of the data sequence, that is, the observation time of the input signal has to be increased.

Though zero padding increases the amount of data to be processed, it has been shown that execution speed for the FFT is the fastest for data sequence of length equals to power of two [6].

The 32 data points are padded with 4,064 zeros in the subsequent discrete time, so as to form a data sequence of length 4,096, which is equal to 2^{12}.

E.   AUTOREGRESSIVE (AR)

The AR model, also known as linear prediction model, predicts the present value of a received digital signal as a linear combination of past p values. The sampled data sequence data, $x(n)$, can be written as

$$x(n) = -\sum_{i=1}^{p} a_i x(n-1) + Gu(n) + G\sum_{l=1}^{q} b_l u(n-1) \tag{4}$$

where a_i and b_l are constants, G is the gain of the system, and $u(n)$ represents white noise [4].

The power spectrum, $P_{AR}(f)$, can be generated using the following equation:

$$P_{AR}(f) = \left| H(e^{j2\pi f t_s}) \right|^2 = \frac{\sigma^2}{\left| 1 + \sum_{i=1}^{p} a_i e^{-j2\pi f} \right|^2} \tag{5}$$

where t_s is the discrete sampling time sequence, $H(e^{j2\pi f t_s})$ is the transfer function, σ is the noise power, and $G = \sigma^2$. The spectrum generated will be narrowband, and the processing to obtain the constants a_i is linear.

The power spectrum of the test signal from Eq. (1) is generated using the AR method. The order, p, of the process is set to be 14, 20, and 30 in Figure 3, Figure 4, and Figure 5 respectively. In Figure 3 where p is 14, a sharp peak is formed at 20.5 MHz, but the two closely-spaced frequencies 36 MHz and 38 MHz are not distinguishable as in the case of the FFT.
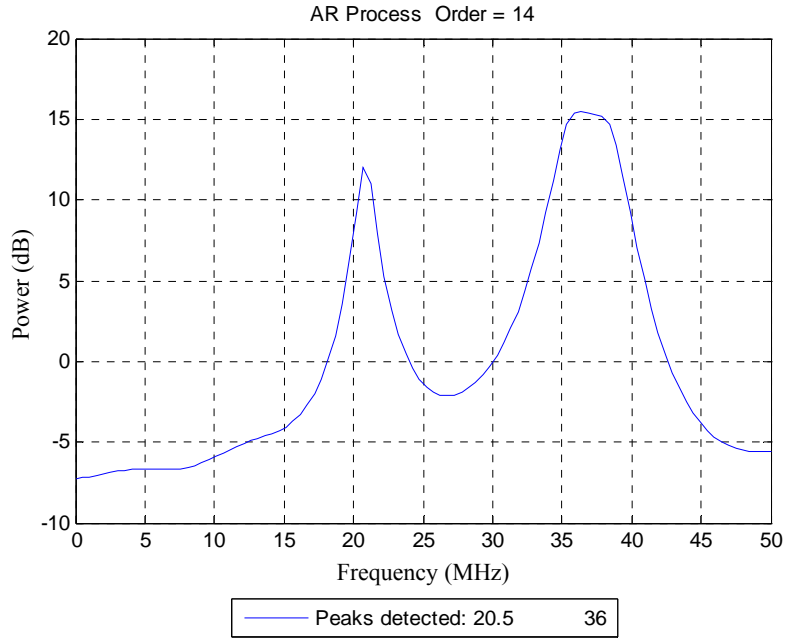
Figure 3.   Spectrum Using AR for *p* = 14.

In Figure 4 where *p* is 20, the two closely-spaced frequencies can be differentiated. As the peaks are not well-defined, the frequencies might not be detected in the presence of noise.
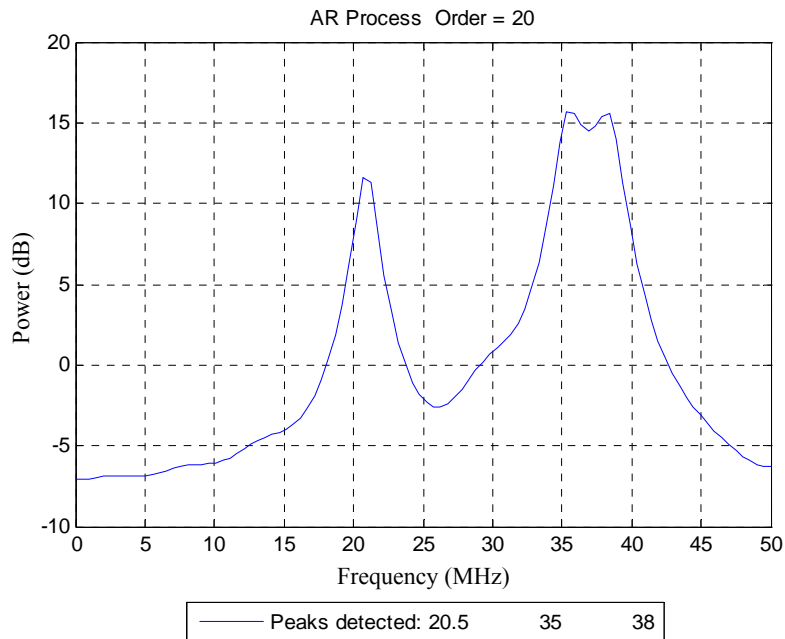
Figure 4.   Spectrum Using AR for *p* = 20.

In Figure 5 where p is 30, the signal is distorted. A frequency is falsely detected in between the two closely-spaced frequencies at 36.5 MHz, and a total of 4 frequencies are detected.
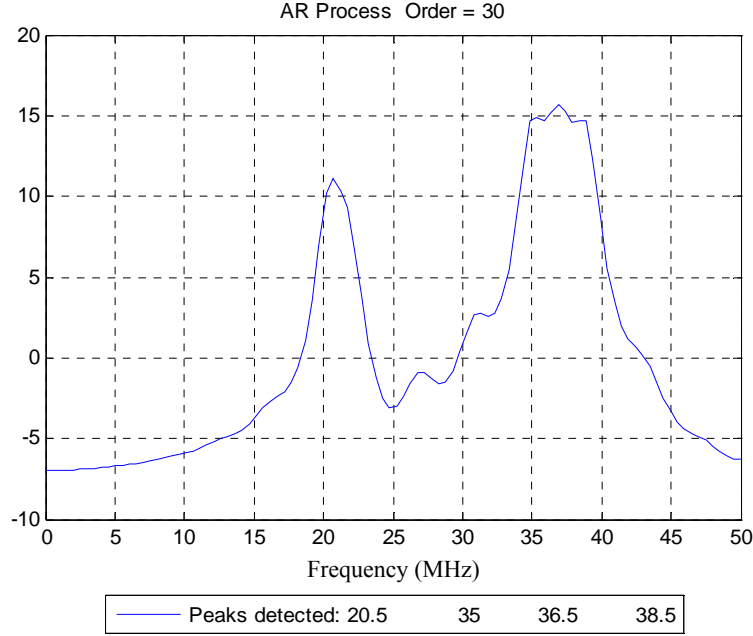
Figure 5.   Spectrum Using AR for p = 30.

From the three spectra, signals with frequencies close together may not be differentiated when the order of the process, p, is low. However, spurious signals may appear when p is set to be too high. Thus, it is critical that the correct value of p is used in order to estimate the inherent frequencies accurately.

F.   MULTIPLE SIGNAL CLASSIFICATION (MUSIC)

The basic idea of the MUltiple SIgnal Classification (MUSIC) method is to separate the signal from the noise in the received signal through eigenvalue decomposition of the autocorrelation matrix, R. The eigendecomposition leverages on the orthogonal property of the signal and noise subspace [4]. R can be written as

$$\begin{pmatrix} R(0) & R(1)^* & ... & R(p)^* \\ R(1) & R(0) & ... & R(p-1)^* \\ ... & & & ... \\ R(p) & R(p-1) & ... & R(0) \end{pmatrix} \tag{6}$$

where $R(k)$ is the autocorrelation of $x(t)$ with lag k as follows:

$$R(k) = E[x(i+k)x(i)^*] \tag{7}$$

and E[.] denotes expectation.

Using eigendecomposition, R can be expressed as

$$RV = \begin{pmatrix} R(0) & R(1)^* & ... & R(p)^* \\ R(1) & R(0) & ... & R(p-1)^* \\ ... & & & \\ R(p) & R(p-1) & ... & R(0) \end{pmatrix} \begin{pmatrix} v_{00} & v_{01} & ... & v_{0p} \\ v_{10} & v_{11} & ... & v_{1p} \\ ... & & & \\ v_{p0} & v_{p0} & ... & v_{pp} \end{pmatrix}$$

$$= \begin{pmatrix} \lambda_0 v_{00} & \lambda_1 v_{01} & ... & \lambda_p v_{0p} \\ \lambda_0 v_{10} & \lambda_1 v_{11} & ... & \lambda_p v_{1p} \\ ... & & & \\ \lambda_0 v_{p0} & \lambda_1 v_{p0} & ... & \lambda_p v_{pp} \end{pmatrix} \tag{8}$$

where V consists of eigenvectors in its columns, and the corresponding eigenvalues are $\lambda_0, \lambda_1, ..., \lambda_p$. If there are M frequencies in the received signal, the first M eigenvalues $\lambda_0, \lambda_1, ..., \lambda_{M-1}$ correspond to the M frequencies, and the rest of the eigenvalues $\lambda_M, \lambda_1, ..., \lambda_p$ correspond to the noise.

The relationship between the different eigenvalues is as follows:

$$\lambda_0 > \lambda_1 > ... > \lambda_{M-1} > \lambda_M = \lambda_{M+1} = ... = \lambda_p = \sigma^2 \tag{9}$$

where σ^2 is the noise power. Using this relationship, the number of frequencies in the received signal can be estimated. The accuracy of this estimation can be undermined by the presence of noise.

The first M eigenvectors that correspond to the M signals form the signal subspace, and are written as V_s. The rest of the eigenvectors that correspond to the noise form the noise subspace, and are written as V_n. That is, $V = [V_s | V_n]$, and V_s and V_n are written as

$$V_s = \begin{pmatrix} v_{00} & v_{01} & \cdots & v_{0(M-1)} \\ v_{10} & v_{11} & \cdots & v_{1(M-1)} \\ \cdots & & & \\ v_{p0} & v_{p0} & \cdots & v_{p(M-1)} \end{pmatrix} \qquad V_n = \begin{pmatrix} v_{0M} & v_{0(M+1)} & \cdots & v_{0p} \\ v_{1M} & v_{1(M+1)} & \cdots & v_{1p} \\ \cdots & & & \\ v_{pM} & v_{p(M+1)} & \cdots & v_{pp} \end{pmatrix} \qquad (10)$$

Since the signal subspace is orthogonal to the noise subspace, the power spectrum, $P_{MUS}(f)$, of the input signal can be generated with

$$P_{MUS}(f) = \frac{1}{s V_n V_s^H s^H} \qquad (11)$$

where s is the data sequence sampled from the received signal, and superscript H is the hermitian of a matrix. Hermitian of a matrix is the transpose and conjugate of that matrix.

To generate $P_{MUS}(f)$, the number of signals M and the order of the filter, p, must be determined. The value of p must be equal to or greater than $2M + 1$. The use of the default value of $p = 2N/3$ is proposed, where N is the number of data points of the received signal [4].

In Figure 6, the power spectrum of the test signal from Eq. (1) is generated using the MUSIC method. There are three frequencies in the test signal, and the number of signals, M, is correctly set to three. The order of the filter, p, is set to the minimum value of $2M + 1 = 7$. The spectrum correctly identifies the three frequencies in the test signal with sharp peaks. The peaks are more defined than those generated using the AR method.
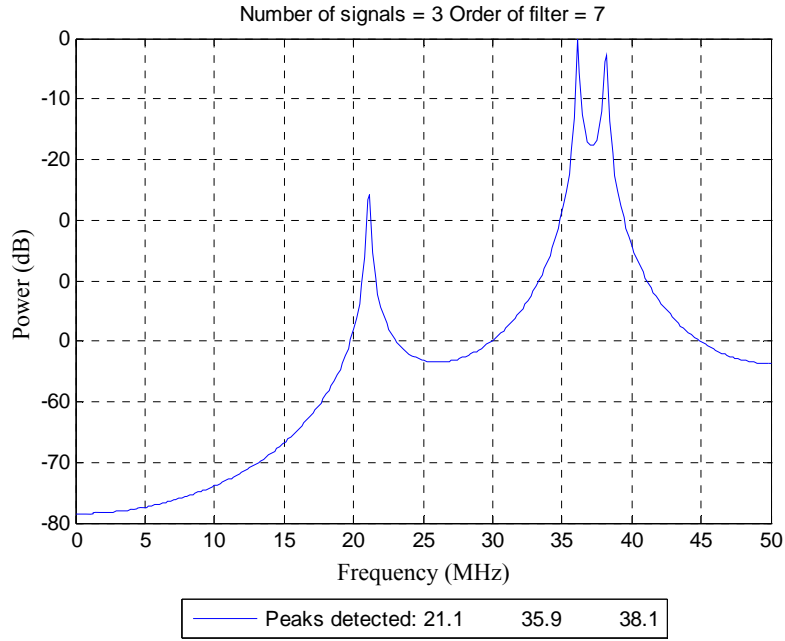
Figure 6.   Spectrum Using MUSIC for $M = 3$ and $p = 7$.

To measure the effects on the MUSIC when the input M value is not correct, M is set incorrectly to be 4 (instead of 3). In Figure 7 and Figure 8, p is set to 9 and 27, respectively. Similarly, the spectrum generated distinctly represents the three frequencies with sharp peaks.

16
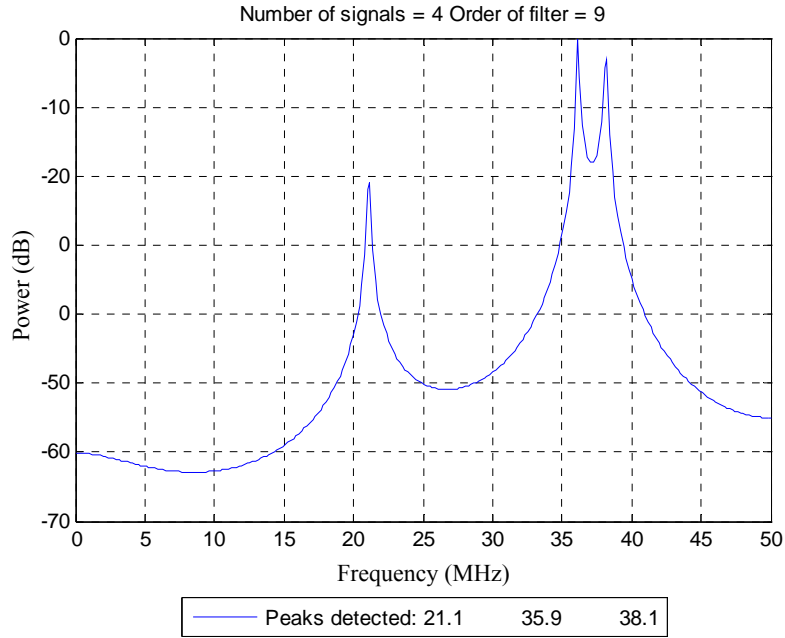
Figure 7.   Spectrum Using MUSIC for $M = 4$ and $p = 9$.
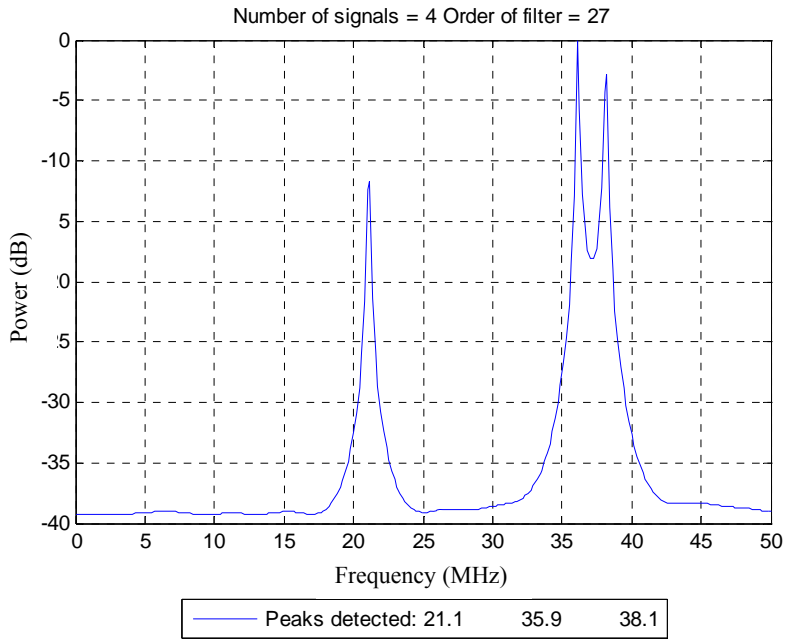
Figure 8.   Spectrum Using MUSIC for $M = 4$ and $p = 27$.

17

When p is increased to 28 in Figure 9, the MUSIC fails to detect the two closely spaced frequencies. A high sharp peak is formed at 21 MHz, and a low broad peak is formed at about 36.1 MHz.
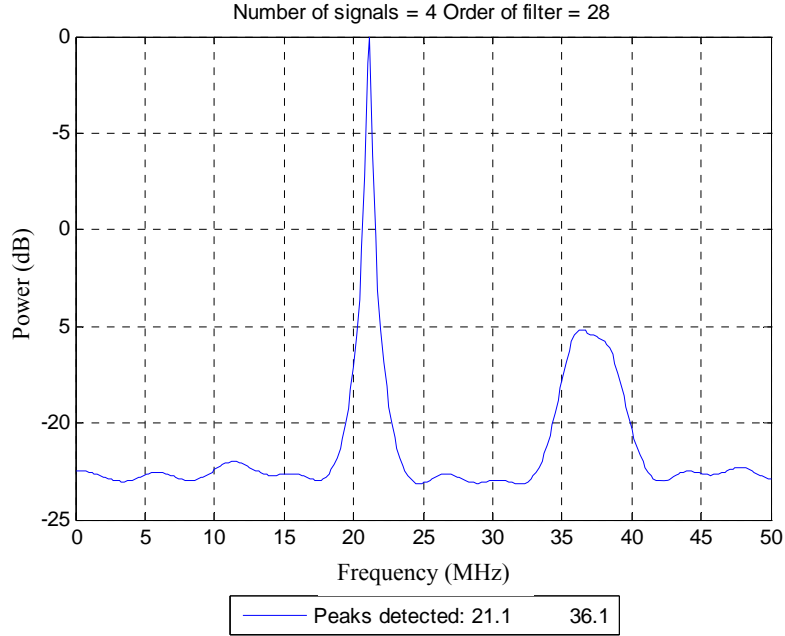
Figure 9. Spectrum Using MUSIC for $M = 4$ and $p = 28$.

In Figure 10, M is set incorrectly at 7 (instead of 3) and p is set to the minimum value of $2M + 1 = 15$. The spectrum depicts four peaks, thus falsely detecting a frequency at 8.8 MHz in the test signal.

Number of signals = 7 Order of filter = 15

Peaks detected: 8.8   21.1   35.9   38.1
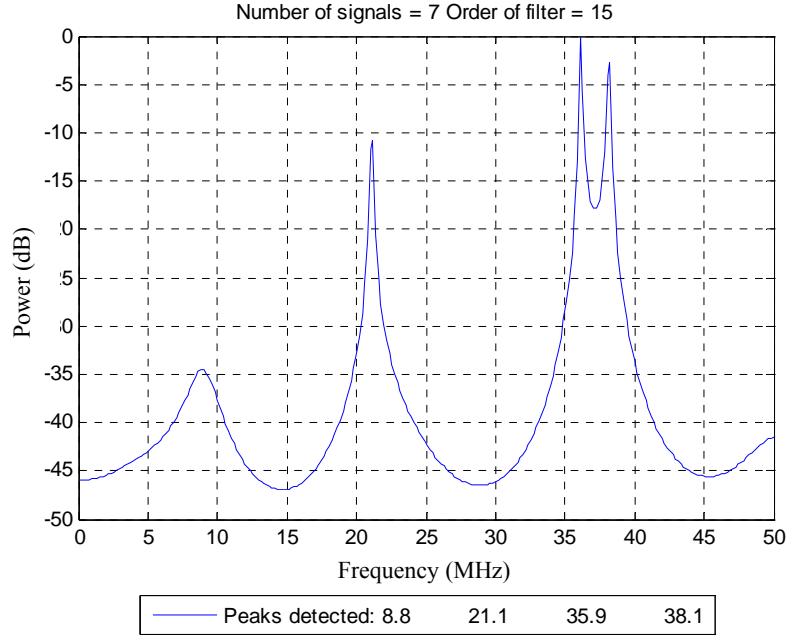
Figure 10.   Spectrum Using MUSIC Method: $M = 7$ and $p = 15$.

In Figure 11, M is set incorrectly at 2 (instead of 3), and p is set to the minimum value of $2M + 1 = 5$. The spectrum detects two frequencies, and fails to distinct the two closely spaced frequencies.

Number of signals = 2 Order of filter = 5

Peaks detected: 21.5   37.1
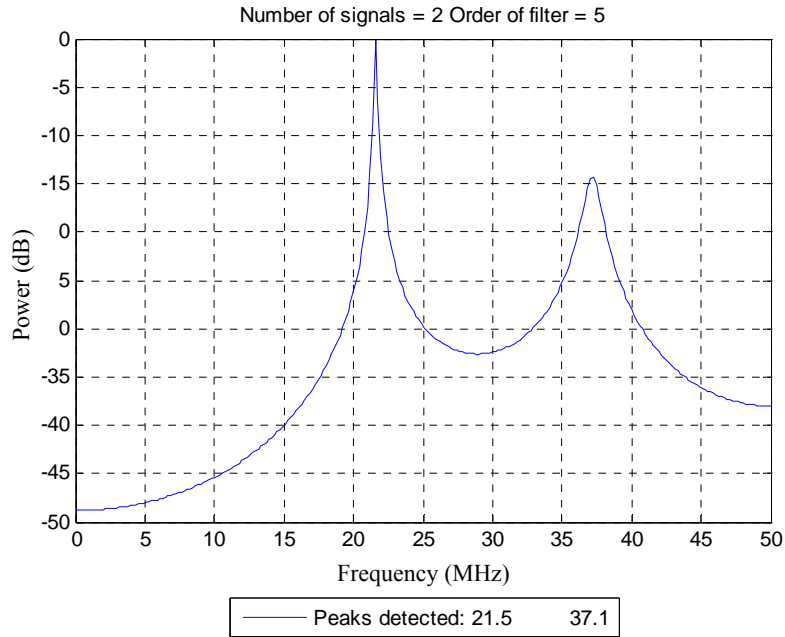
Figure 11.   Spectrum Using MUSIC for $M = 2$ and $p = 5$.

From the simulated results, it can be observed that the accuracy of the MUSIC method in detecting the inherent frequencies of the test signal is less dependent on the order of the filter, p. When p varies from 9 to 27, the spectrum shows three sharp peaks to represent the three frequencies of the test signal.

However, an accurate value of M has to be input into the MUSIC algorithm in order to generate a correct spectrum. When M is increased from 3 to 6, spurious signal appears in the spectrum and results in false detection. When M is reduced from 3 to 2, the two closely-spaced frequencies are detected as a single frequency. Therefore, for MUSIC to accurately detect the frequencies in a received signal, it is critical that the number of frequencies is accurately determined from Eq. (9) or other means.

G. ESTIMATION OF SIGNAL PARAMETERS VIA ROTATIONAL INVARIANCE TECHNIQUES (ESPRIT)

Unlike AR and MUSIC methods, the Estimation of Signal Parameters via Rotational Invariance Techniques (ESPRIT) does not search the entire frequency range for peaks in the power spectrum. However, the ESPRIT method performs the eigendecomposition twice, thus it is computationally more intensive than the AR and MUSIC methods [4]. Similar to MUSIC method, the number of frequencies in the input signal must be determined correctly, so that the frequency components can be identified accurately.

The input signal is sampled, and is represented as $x(n)$, where $n=0, 1,…, N\text{-}1$. Two data series, G_1 and G_2, are written based on $x(n)$ as

$$G_1 = x(0), x(1),..., x(n-2)$$
$$G_2 = x(1), x(2),..., x(n-1)$$

(12)

The order of the filter, p, is set to be $\dfrac{N}{2}-1$. With an even number of samples (i.e. N is even), the autocorrelation matrix, R_{yy}, and cross-correlation matrix, R_{yz}, are formed as

$$R_{yy} = yy^H = y((y)^T)^* \qquad\qquad R_{yz} = yz^H = y((z)^T)^*$$

(13)

where the superscript H is the hermitian operation, T is the transpose operation, $*$ is the conjugate operation, and

$$
y = \begin{bmatrix}
x(0) & x(1) & \cdots & x(\frac{N}{2}-1) \\
x(1) & x(2) & \cdots & x(\frac{N}{2}) \\
\vdots & \vdots & \vdots & \vdots \\
x(\frac{N}{2}-1) & x(\frac{N}{2}) & \cdots & x(N-2)
\end{bmatrix}_{\frac{N}{2}\times\frac{N}{2}} ,
$$

$$(14)$$

$$
z = \begin{bmatrix}
x(1) & x(2) & \cdots & x(\frac{N}{2}) \\
x(2) & x(3) & \cdots & x(\frac{N}{2}+1) \\
\vdots & \vdots & \vdots & \vdots \\
x(\frac{N}{2}) & x(\frac{N}{2}+1) & \cdots & x(N-1)
\end{bmatrix}_{\frac{N}{2}\times\frac{N}{2}}
$$

Eigendecomposition is performed on R_{yy} as

$$
R_{yy}e' = \lambda'e'
$$

$$(15)$$

to obtain e' and λ', which are the eigenvectors and eigenvalues respectively. Similar to the MUSIC operation in Eq. (9), the number of frequencies, M, in the received signal can be estimated by processing e' and λ'.

Using the smallest eigenvalue λ_{min} from λ', matrices R_s and R_t are formed as

$$
R_s = R_{yy} - \lambda_{min}I \qquad\qquad R_t = R_{yz} - \lambda_{min}D
$$

$$(16)$$

where

$$
I = \begin{bmatrix}
1 & 0 & 0 & \cdots & 0 \\
0 & 1 & 0 & \cdots & 0 \\
0 & 0 & 1 & \cdots & 0 \\
\vdots & \vdots & \vdots & \ddots & \vdots \\
0 & 0 & 0 & \cdots & 1
\end{bmatrix}_{\frac{N}{2}\times\frac{N}{2}}
\qquad
D = \begin{bmatrix}
0 & 0 & \cdots & 0 & 0 \\
1 & 0 & \cdots & 0 & 0 \\
0 & 1 & \cdots & 0 & 0 \\
\vdots & \vdots & \ddots & \vdots & \vdots \\
0 & 0 & \cdots & 1 & 0
\end{bmatrix}_{\frac{N}{2}\times\frac{N}{2}}
$$

$$(17)$$

The generalized eigendecomposition of R_s and R_t is

$$R_s e = \lambda R_t e \tag{18}$$

where e and λ are the eigenvector and eigenvalue. The λ values close to the unit circle are determined. The values are then used to determine the frequency components of the input signal, given by

$$f_i = \frac{1}{2\pi} \tan^{-1}\left(\frac{\operatorname{Im} \lambda_i}{\operatorname{Re} \lambda_i}\right) \tag{19}$$

The test signal from Eq. (1) is analyzed using the ESPRIT method with the order of filter, p, set to be $N/2$. Similar to the MUSIC method, the number of frequencies, M, in the test signal has to be determined and input into the ESPRIT method. To evaluate the performance of ESPRIT method, the value of M is varied, and the results are tabulated in Table 1. It is observed that the accuracy of ESPRIT is highly dependent on the accuracy of M. When the correct number of frequencies is input into the ESPRIT method, the three frequencies at 21 MHz, 36 MHz, and 38 MHz are correctly detected. When the number of frequencies is under-estimated, $(3 - M)$ frequencies of the test signal are not detected. When the number of frequencies is over-estimated, one frequency is falsely detected at 50 MHz.

Table 1.   Frequencies Detected Using ESPRIT for $M = 1, 2, \ , 6$.

Number of Frequencies, M	Frequencies detected / MHz	Frequencies Not Detected / MHz	Frequencies Falsely Detected
1	21	36, 38	-
2	21, 36	38	-
3	21, 36, 38	-	-
4	21, 36, 38, 50	-	50
5	21, 36, 38, 50	-	50
6	21, 36, 38, 50		50

H.   MINIMUM NORM

Similar to the MUSIC method, the Minimum Norm method calculates the signal subspace, V_s, and the noise subspace, V_n, as in Eq. (10) [4]. V_n is rewritten as

$$V_n = \begin{pmatrix} v_{0M} & v_{0(M+1)} & \cdots & v_{0p} \\ v_{1M} & v_{1(M+1)} & \cdots & v_{1p} \\ \cdots & & & \\ v_{pM} & v_{p(M+1)} & \cdots & v_{pp} \end{pmatrix} = \begin{pmatrix} c^H \\ V_n' \end{pmatrix} \qquad (20)$$

where the superscript H is the hermitian operation, c^H is the first row of V_n, and V_n' contains the rest of the rows of V_n. They are written as

$$c^H = \begin{bmatrix} v_{0M} & v_{0M+1} & \cdots & v_{0p} \end{bmatrix} \qquad V_n' = \begin{bmatrix} v_{1M} & v_{1M+1} & \cdots & v_{0p} \\ \vdots & \vdots & \cdots & \vdots \\ v_{pM} & v_{pM+1} & \cdots & v_{pp} \end{bmatrix} \qquad (21)$$

A vector, d, which is a linear combination of eigenvectors in the noise subspace, is calculated as

$$d = \frac{1}{V_n' c / (c^H c)} \qquad (22)$$

where the square of the norm of d, $|d|^2 = \sum_{i=0}^{p} d_i^2$, is minimized.

The power spectrum $P_{MN}(f)$ of the input signal can then be defined as

$$P_{MN}(f) = \frac{1}{s d d^H s^H} \qquad (23)$$

where s is assumed to be the input vector

$$s = \begin{bmatrix} 1 & e^{-j2\pi f} & \cdots & e^{-j2\pi(N-1)f} \end{bmatrix} \qquad (24)$$

The test signal from Eq. (1) is analyzed using the Minimum Norm method. The number of signals, M, is correctly set to 3, and the order of filter, p, is set to be 20. The spectrum of the input signal is plotted in Figure 12. The results are similar to the MUSIC method, except that there are a few low lying peaks. These low-lying peaks might result in false detection if the threshold is not properly set or if the noise is significant.
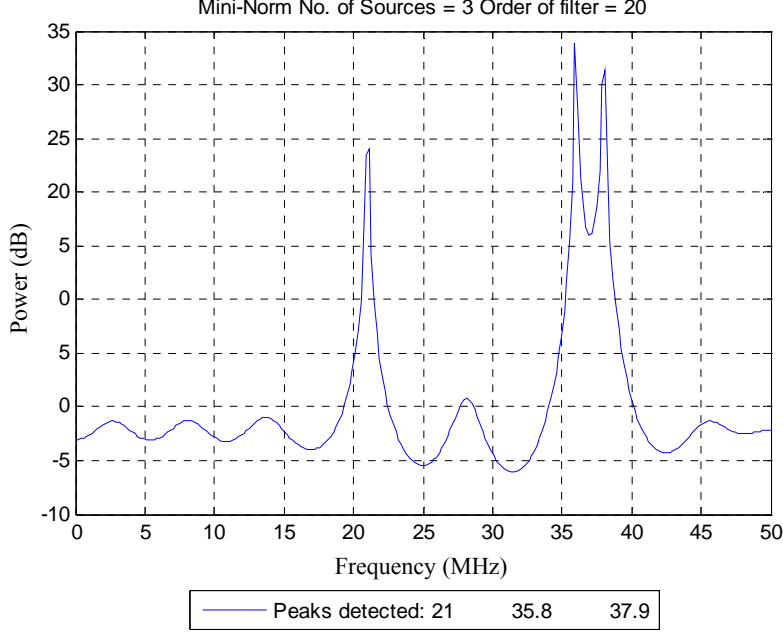
Figure 12.   Spectrum Using Minimum Norm for $M = 3$ and $p = 20$.

I.   MULTI-RESOLUTION SPECTRUM SENSING (MRSS)

A wideband dual-stage multi-resolution spectrum sensing (MRSS) technique was proposed for cognitive radio systems [7]. A coarse sensing is performed over a large frequency range in a short time to provide a low resolution spectrum. The frequency search is then narrowed down to segments of the spectrum where the energy levels are higher than the threshold level, thus indicating signals being transmitted in those segments. For these identified segments, the fine sensing is used to estimate the frequency components of the received signal. The fine sensing takes about 25 times more processing time than the coarse sensing. The difference in processing time is significant when a wide spectrum is searched for the presence of signals.

A functional block diagram of an analog MRSS system is shown in Figure 13. It consists of a wavelet waveform generator, multipliers and integrators, and low speed analog-to-digital converters (ADC). The multipliers and integrators are used to perform correlation. The wavelet acts as a bandpass filter and eliminates unwanted signals and noise outside of the frequency band of interest.

24
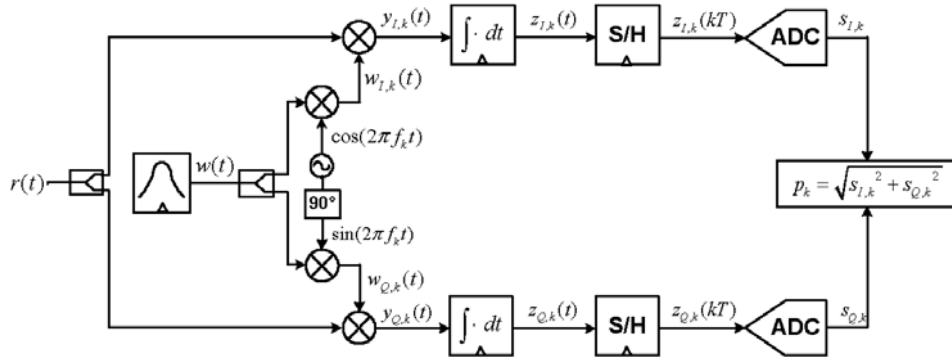
Figure 13.   Functional Block Diagram of an Analog MRSS System (From [7]).

The spectrum of interest is demarcated by its start frequency, f_{start}, and its end frequency, f_{stop}. For coarse sensing, a larger sweep frequency, f_{sweep}, is chosen to provide a lower resolution spectrum. For fine sensing, a smaller sweep frequency, f_{sweep}, is chosen to identify the inherent frequencies of the received signal, $r(t)$.

The locally generated wavelet, $w(t)$, is multiplied with sinusoidal signals from the local oscillators to form $w_{I,k}(t)$ and $w_{Q,k}(t)$ as

$$w_{I,k}(t) = w(t)\cos(2\pi f_k t) \qquad \text{for } k = 0,...,KK \tag{25}$$

$$w_{Q,k}(t) = w(t)\sin(2\pi f_k t) \qquad \text{for } k = 0,...,KK \tag{26}$$

where $KK = \text{floor}\left[(f_{stop} - f_{start})/f_{sweep} \right]$ and $f_k = f_{start} + kf_{sweep}$. Floor[x] is an operation to obtain the next integer lesser than x.

The received signal, $r(t)$, is multiplied with $w_{I,k}(t)$ and $w_{Q,k}(t)$ respectively in the in-phase (I) and quad-phase (Q) channels, before each of them is passed through an integrator. The outputs of the integrators are

$$z_{I,k}(t) = \left(\frac{1}{T_w}\right)\left(\int_{kT_w}^{(k+1)T_w} r(t)w_{I,k}(t)dt \right) \tag{27}$$

$$z_{Q,k}(t) = \left(\frac{1}{T_w}\right)\left(\int_{kT_w}^{(k+1)T_w} r(t)w_{Q,k}(t)dt \right) \tag{28}$$

25

The analog-to-digital converter (ADC) in each channel samples $z_{I,k}(t)$ and $z_{Q,k}(t)$ at a period of T_w to form the digital signals $s_{I,k}(t)$ and $s_{Q,k}(t)$ as follows:

$$s_{I,k} = z_{I,k}\left(kT_w\right) \tag{29}$$

$$s_{Q,k} = z_{Q,k}\left(kT_w\right) \tag{30}$$

The spectral density at frequency f_k is given by

$$p_k = \sqrt{s_{I,k}^2 + s_{Q,k}^2} \tag{31}$$

The total processing time, T_{total}, for spectrum sensing is inversely proportional to the window bandwidth (or the width of the spectrum of interest), B_w, and f_{sweep} as shown

$$T_{total} = T_w \times KK \propto \frac{1}{B_w}\frac{1}{f_{weep}} \tag{32}$$

The test signal from Eq. (1) is analyzed using the MRSS method. As highlighted in Eq. (1), the test signal is sampled 32 times and has $N = 32$ data points. With f_{sweep} set to 0.02 MHz, i.e., 1/100 of the smallest frequency spacing of 2 MHz in the test signal's spectrum, the power spectrum of the test signal is generated using MRSS and is plotted in Figure 14. The two broad peaks represent the two frequencies that are detected. The MRSS is not able to differentiate the two closely spaced frequencies.
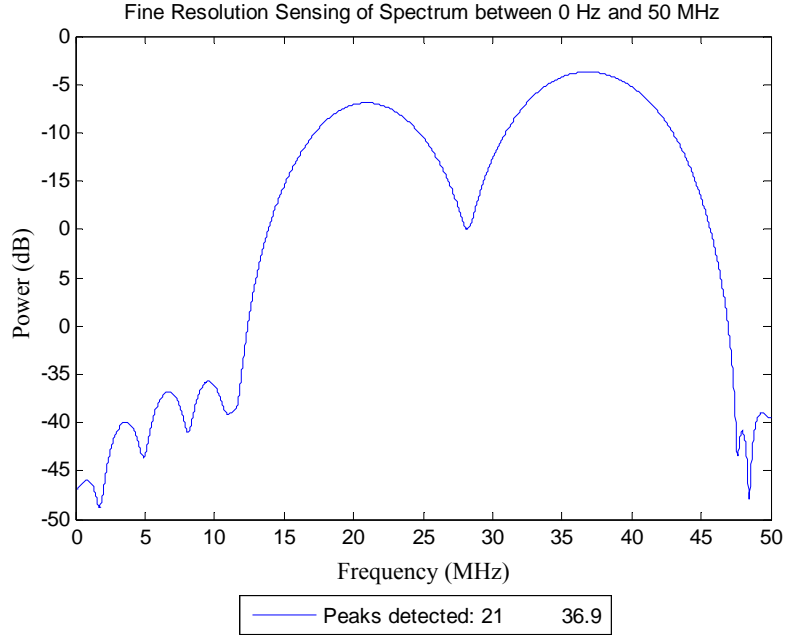
Figure 14.　　Spectrum Using MRSS for $N = 32$ and $f_{sweep} = 0.02$ MHz.

The sweep frequency, f_{sweep}, is reduced by a factor of 10 to 0.002 MHz, i.e. 1/1000 of the smallest frequency spacing of 2 MHz in the test signal's spectrum. A plot of the spectrum is shown in Figure 15. Despite increasing the sweep resolution by a factor of 10, the spectrum remains the same, and the two closely spaced frequencies remain undifferentiated.
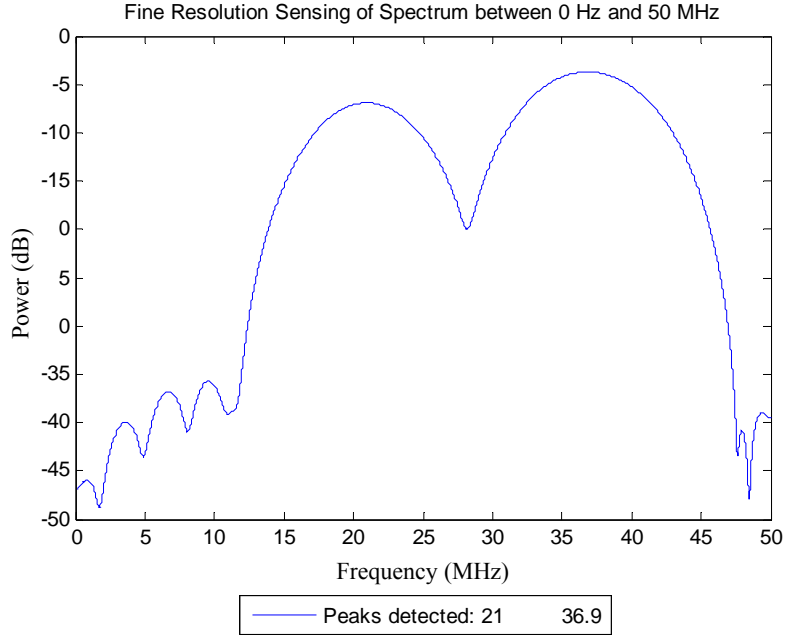
Figure 15.   Spectrum Using MRSS for $N = 32$, and $f_{sweep} = 0.002$ MHz.

With f_{sweep} set to the original 0.02 Hz, the number of data points, N, is increased by a factor of 2, and the spectrum is plotted in Figure 16. With 64 data points, the MRSS is now able to differentiate the two closely spaced frequencies, though the two peaks are not very pronounced. Furthermore, the peaks have narrower bases and are more distinct.
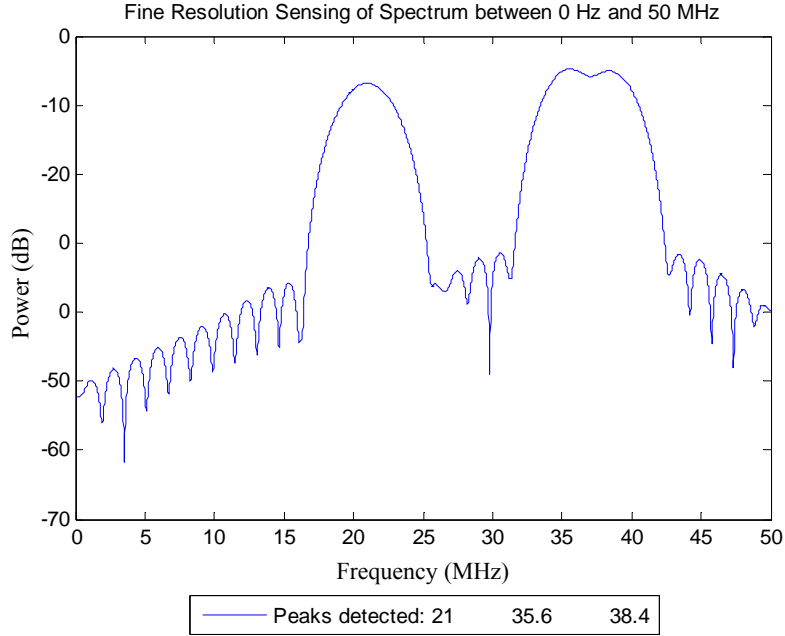
Figure 16.   Spectrum Using MRSS for $N = 64$, and $f_{sweep} = 0.02$ MHz.

The number of data points, N, is increased to 320, 512 and 3200, and the respective spectra are plotted in Figures 17, 18 and 19. As N increases, the peaks become narrower and more defined. The sidelobes between the two closely spaced frequencies also decrease allowing for more accurate frequency estimation. The minimum signal power decreases by 20 dB from -80 dB to -100 dB as N increases by 10 times from 320 to 3200, thus increasing the heights of the peaks.
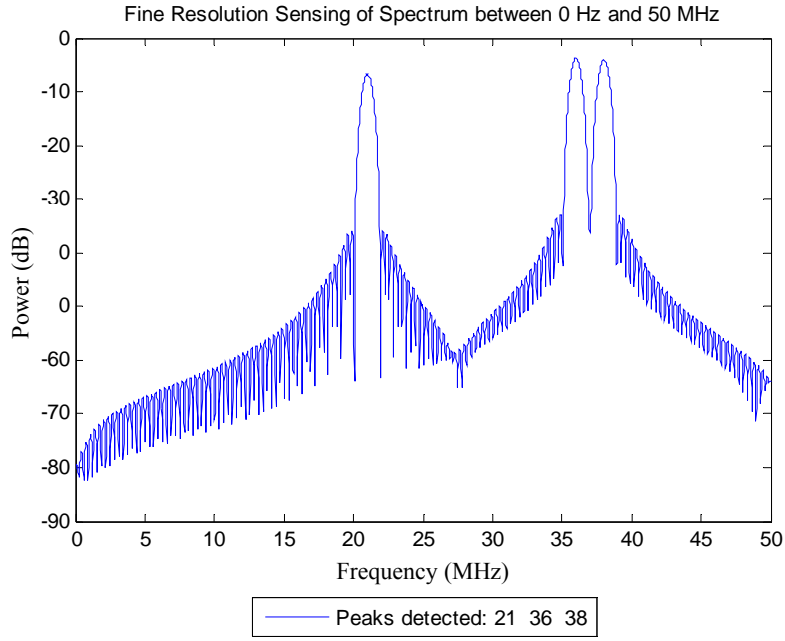
Figure 17.   Spectrum Using MRSS for $N = 320$, and $f_{sweep} = 0.02$ MHz.
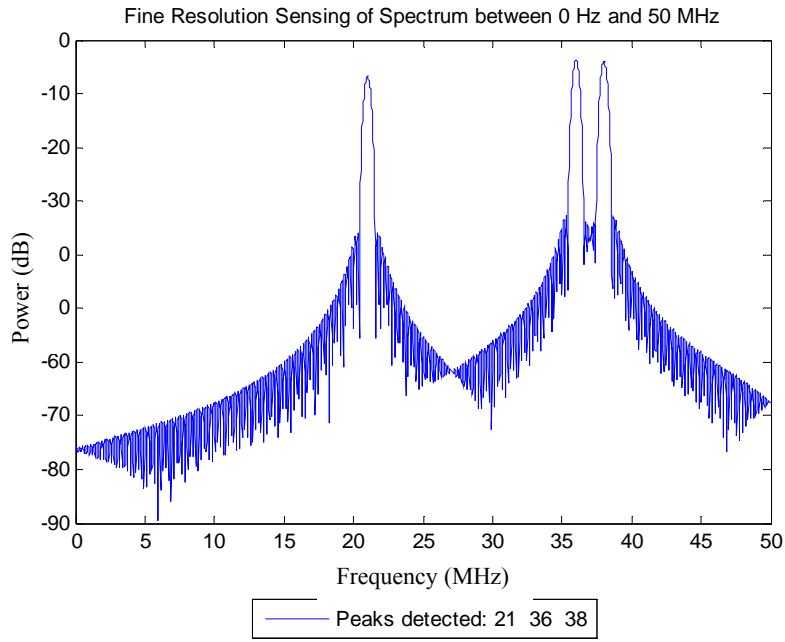
Figure 18.   Spectrum Using MRSS for $N = 512$, and $f_{sweep} = 0.02$ MHz.
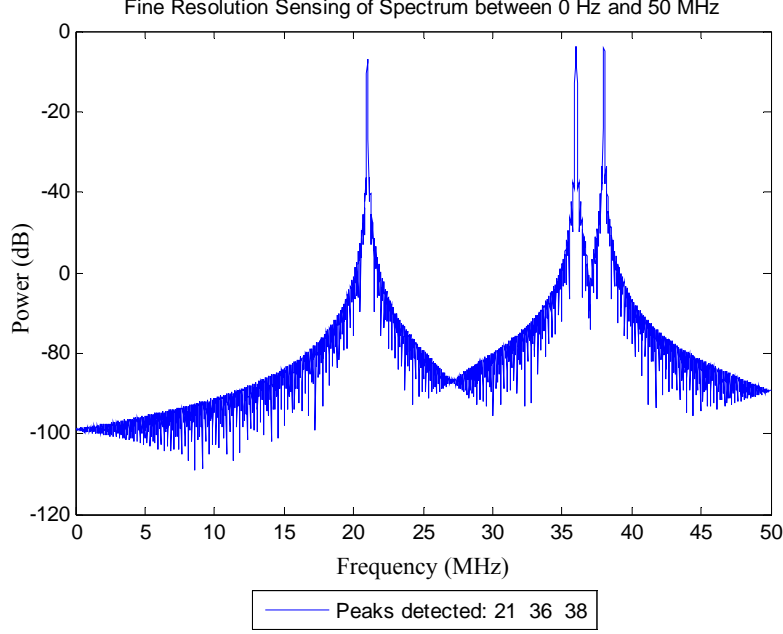
Figure 19.　　　Spectrum Using MRSS for $N = 3200$, and $f_{sweep} = 0.02$ MHz.

J.　SUMMARY

The FFT does not provide the required resolution in the power spectrum generated, thus high resolution spectrum estimation methods are used. Using the input test signal from Eq. (1), the AR method is shown to depend heavily on the order, p, and the peaks in the spectrum are not pronounced. The MUSIC is less sensitive to order of the filter, p, and displays sharp peaks in the spectrum. However, it is dependent on the accuracy of the number of frequencies, M, in the signal. Unlike the MUSIC, the ESPRIT does not search the entire frequency range for peaks in the power spectrum. It offers very accurate results in a noiseless environment. Like the MUSIC, the ESPRIT is also dependent on the accuracy of M. The minimum norm method produces results similar to that of the MUSIC, except that the low lying peaks in the power spectrum might result in false detection in the presence of noise. The MRSS provides accurate spectrum estimation, but it requires a longer observation time. The three distinct methods, namely, MUSIC, ESPRIT, and MRSS, are chosen for further analysis in the subsequent chapters.

31

THIS PAGE INTENTIONALLY LEFT BLANK

III. IMPLEMENTATION OF A SPECTRUM ESTIMATOR

The first section of this chapter provides an overview of processing a received signal before applying a high resolution spectrum estimation method. In Section B, an analog received signal is defined with multi-tone spectrum to test the performance of the various spectrum estimation methods. In Section C, a frequency down-conversion mixer circuit is presented. In Section D, the received signal defined in Section B is converted down to baseband frequency. The last section demonstrates the need of a bandpass filter prior to the mixer circuit, so as to eliminate false detection due to frequencies outside the band of interest. The FFT is used to show the spectrum of the digitized output signal in all the sections.

A. INTRODUCTION

A spectrum estimation module of a digital receiver is built and simulated with an analog received signal. The received signal is first down-converted to baseband frequency. It is further demonstrated that the received signal has to pass through a bandpass filter before it is down-converted, so that there are no ambiguities and false detections caused by frequencies outside the band of interest. After the received signal is bandpassed and down-converted, the analog signal is converted to digital form using an analog-to-digital converter (ADC), so that high resolution spectrum estimation methods can be used to determine the inherent frequencies of the received signal in the specific band of interest.

B. INPUT TEST SIGNAL

To rigorously test and evaluate the performance of the spectrum estimation module, an analog received signal with multi-tone spectrum is generated and input into the module. The simulated received signal is

$$r(t) = +1.3\cos\left(2\pi 2.410\times 10^9 t + 0.1\right) + 2\cos\left(2\pi 2.411\times 10^9 t\right)$$
$$+1.5\cos\left(2\pi 2.4300\times 10^9 t + 0.2\right) + 1.9\left(2\pi 2.4305\times 10^9 t\right) \tag{33}$$
$$+1.4\cos\left(2\pi 2.4400\times 10^9 t + 0.3\right) + 1.8\cos\left(2\pi 2.4401\times 10^9 t\right)$$

The received signal, $r(t)$, is a combination of seven sinusoidal signals, which have different amplitudes and phases. The frequencies are 2.410 GHz, 2.411 GHz, 2.4300 GHz, 2.4305 GHz, 2.4400 GHz and 2.4401 GHz. The six frequencies can be grouped into three pairs of frequencies with 1 MHz, 0.5 MHz, and 0.1 MHz spacing respectively. One of the performance criteria of a spectrum estimation method is its spectral resolution. That is, the ability to distinguish one frequency from another in each pair of frequencies.

The spectrum of interest is from 2.4 GHz to 2.45 GHz, that is, the bandwidth of interest is 50 MHz. According to Nyquist theorem, the bandwidth is ½ of the sampling frequency, f_s, of the ADC. This thesis assumes that a medium-range commercial ADC, which operates at a maximum sampling rate of 100 MHz, is used. Hence, the bandwidth of interest, B, is

$$B = \frac{1}{2}f_s = \frac{1}{2}\times 100 \times 10^6 = 50\,\mathrm{MHz} \tag{34}$$

The signal, $r(t)$, is captured over an observation window of 1 μs. As the analog received signal is simulated using MATLAB, a high sampling rate of 10 GHz is used to generate the analog signal.

C. SINGLE CHANNEL FREQUENCY DOWN-CONVERTER CIRCUIT

A mixer is utilized to convert the frequency range of the receiver signal to baseband for the ease of signal processing [4]. A frequency down-converter circuit is shown in Figure 20. The output signal of the mixer, $y(t)$, is given by

$$y(t) = r(t) \times c(t) \tag{35}$$

where $r(t)$ is the received signal to be demodulated and $c(t)$ is the local oscillator (LO) signal.
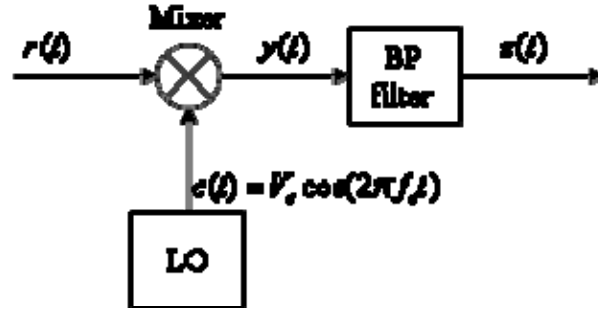
Figure 20.   Single Channel Frequency Down-Converter Circuit (After [4]).

A mixer is a nonlinear device, and its output signal current, I, can be related to its input signal voltage, V, by

$$I = a_0 + a_1 V + a_2 V^2 + ... \tag{36}$$

where a_0, a_1, a_2,... are constants. The nonlinear linear relationship between I and V is plotted in Figure 21.
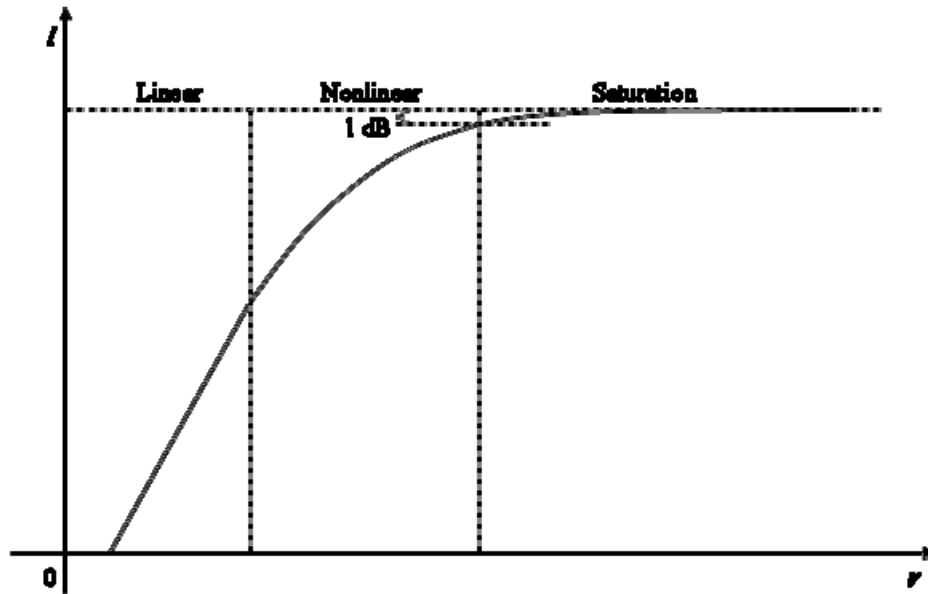
Figure 21. I - V Nonlinear Relationship of a Mixer.

Assuming that the received signal, $r(t)$ has a single frequency, f_r, and amplitude, V_r, and the local oscillator signal, $c(t)$, has a frequency, f_c, and amplitude, V_c, the input signal into the mixer is

$$V = r(t) + c(t) = V_r \sin(2\pi f_r t) + V_c \sin(2\pi f_c t) \tag{37}$$

Substituting Eq. (37) into the $a_2 V^2$ term in Eq. (36), the corresponding part of the signal, $y(t)$, is

$$a_2 V^2 = a_2 V_r^2 \sin^2(2\pi f_r) + a_2 V_c^2 \sin^2(2\pi f_c)$$
$$+ a_2 V_r V_c \left\{ \cos\left[2\pi (f_r - f_c) t \right] - \cos\left[2\pi (f_r + f_c) t \right] \right\} \tag{38}$$

A lowpass filter is implemented to eliminate the noise outside the frequency band of interest. When $y(t)$ is passed through a lowpass filter, the baseband signal is obtained as

$$z(t) = a_2 V_r V_c \cos\left[2\pi (f_r - f_c) t \right] \tag{39}$$

In MATLAB, as a high sampling rate of 10 GHz is used to represent the analog signal, the spectrum of the signal is repeated at every 5 GHz. The lowpass filter will eliminate the repeated spectrum in the higher frequencies. Thus, the integrity of the MATLAB simulated analog signal is preserved.

D.   FREQUENCY DOWN-CONVERSION

Using the simulated analog received signal, $r(t)$, in Eq. (33), the local oscillator signal, $c(t)$, is generated at 2.4 GHz so as to convert the 2.4 GHz to 2.45 GHz portion of the spectrum to the range 0 Hz to 50 MHz. More simply, the entire received signal's spectrum is subtracted and lowered by 2.4 GHz. Due to rolloff in the lowpass filter characteristics, the critical frequency, f_c, of the lowpass filter is set to be 20% larger than the bandwidth of interest, B, at 50 MHz. That is, f_c is set to 120 % × 50 MHz = 60 MHz.

Before the signal can be processed to estimate its spectrum, $z(t)$ is sampled and converted to its digital form using a ADC. A medium-range ADC, which can support up to 100 MHz of sampling rate, is used. In MATLAB, a high sampling rate of 10 GHz is used to represent the analog signal. Thus, the ADC is simulated by reducing the sampling rate to 100 MHz. This is achieved by interpolating every consecutive 100 data points to one point. With an observation window of 1 μs, the digitized received signal, $r(t)$, in baseband frequency has 101 data points.

The FFT of the digitized $z(t)$ is plotted in Figure 22. From the power spectrum plot, the FFT identifies frequencies at 9.4 MHz, 10.9 MHz, 30.5 MHz, and 38.8 MHz. Since the spectrum is previously lowered by 2.4 GHz through mixing, the actual frequencies are calculated by adding 2.4 GHz to each of the frequencies detected. Therefore, the actual frequencies detected are 2.4094 GHz, 2.4109 GHz, 2.4305 GHz, and 2.4388 GHz. The maximum error from the actual frequencies is quite significant at 1.2 MHz. It is noted that the two frequencies spaced at 1 MHz apart can be detected using the FFT. As expected, the frequencies spaced at 0.5 MHz and 0.1 MHz cannot be detected with the FFT. Therefore, high resolution spectrum estimation methods are required.
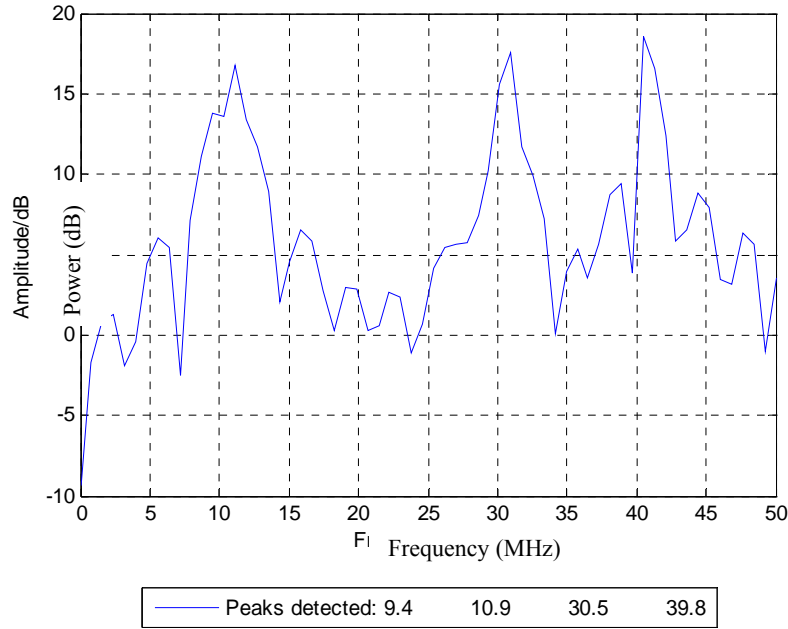
Figure 22.   Spectrum of Digitized Received Signal, $r(t)$, in Baseband Using FFT.

E.   NEED FOR BANDPASS FILTER

To illustrate the need for the received signal to pass through a bandpass filter before mixing, a sinusoidal signal at 2.380 GHz is generated, which is out of the frequency band of interest (2.4 – 2.45 GHz). It is combined with the received signal, $r(t)$, in Eq. (33) to form

$$
\begin{aligned}
r'(t) = {} & \cos\left(2\pi 2.380\times10^9 t + 0.1\right) \\
& +1.3\cos\left(2\pi 2.410\times10^9 t + 0.1\right) + 2\cos\left(2\pi 2.411\times10^9 t\right) \\
& +1.5\cos\left(2\pi 2.4300\times10^9 t + 0.2\right) + 1.9\left(2\pi 2.4305\times10^9 t\right) \\
& +1.4\cos\left(2\pi 2.440\times10^9 t + 0.3\right) + 1.8\cos\left(2\pi 2.4401\times10^9 t\right)
\end{aligned}
\tag{40}
$$

Using the same frequency down-converter circuit in Figure 23, the FFT of the digitized $z(t)$ is plotted in Figure 21. The actual frequencies detected are 2.4094 GHz, 2.4109 GHz, 2.4203 GHz, 2.4305 GHz, and 2.4388 GHz. The frequency 2.380 GHz is falsely detected as 2.420 GHz. This is because both 2.380 GHz and 2.420 GHz are 20 MHz away from the frequency of the local oscillator, f_s. For a single channel down-converter, the frequencies below the local oscillator frequency, f_c, "wrap around" and are indistinguishable from the frequencies above.

One means of preventing false detection of frequencies outside the band of interest, a bandpass filter is implemented at the front of the mixer circuit as shown in Figure 24. Considering that the critical frequency of the lowpass filter is set at 60 MHz, the passband frequencies are set to be 2.400 GHz to 2.460 GHz.
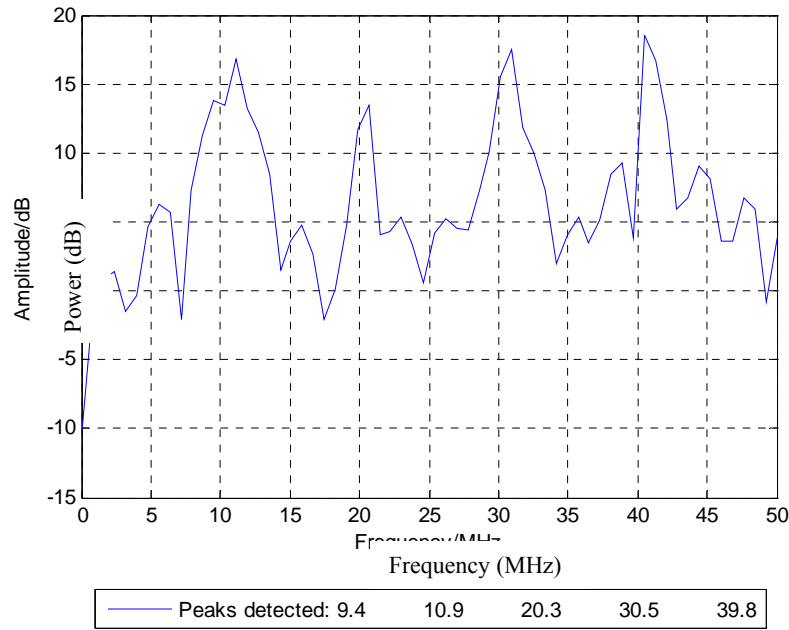
Figure 23.   Spectrum of Digitized Received Signal, $r'(t)$, in Baseband Using FFT.
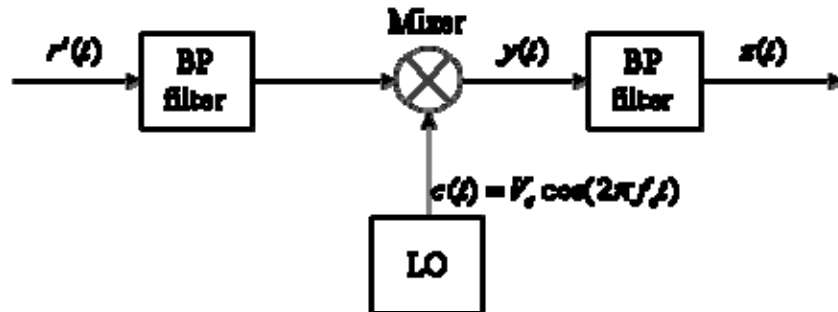
Figure 24.   Single Channel Frequency Down-Converter Circuit With Bandpass Filter.

The FFT of the digitized $z(t)$ is plotted in Figure 25. As the frequencies outside the band of interest are filtered off, there is no false detection. In the MATLAB simulation, a finite impulse response (FIR) filter is used as a bandpass filter. As the transfer function of the FIR filter is not an ideal rectangular function, the spectrum is slightly different from that without the bandpass filter in Figure 21. The peaks in the spectrum are not significantly affected by the bandpass filter.

39
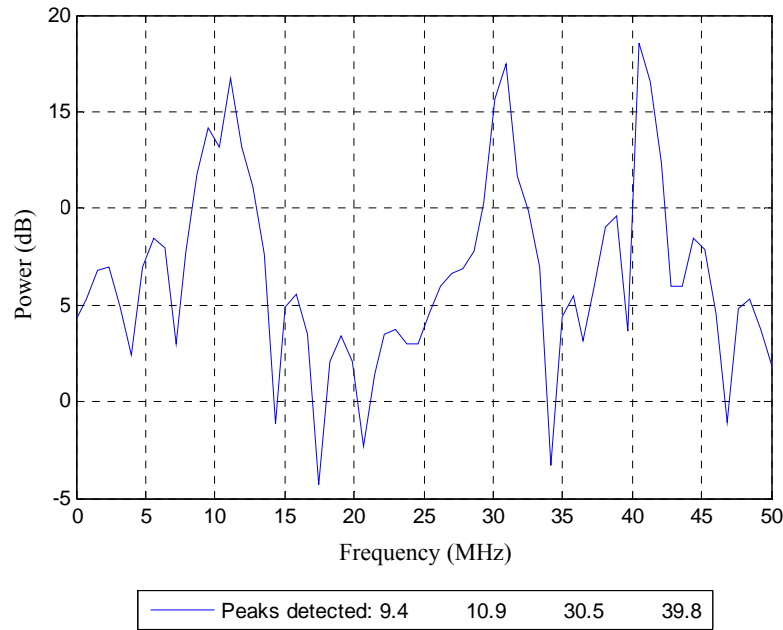
Figure 25.   Spectrum of Digitized Received Signal, $r'(t)$, in Baseband Using FFT and Bandpass Filter.

F.   IN-PHASE (*I*) AND QUAD-PHASE (*Q*) CHANNEL CONVERSION

In the above sections, the bandwidth of interest is limited to half of the maximum sampling rate, f_s, of the ADC. However, the effective bandwidth can be doubled if both an in-phase (*I*) and quad-phase (*Q*) channel (quadrature) is used instead of a single channel frequency down-conversion [4]. According to Nyquist sampling theorem, the minimum sampling rate is twice the highest frequency in the band of interest. With an additional *Q* channel, the number of data samples doubles for a fixed sampling rate. Thus, the bandwidth of interest is also doubled.

An *I* and *Q* channel frequency down-converter circuit is shown in Figure 26. The received signal, $r'(t)$, is split and passed through two bandpass filters simultaneously. Unlike the single channel converter, the bandpass filters have bandwidths of f_s (instead of $f_s/2$) centered at the carrier frequency, f_c. The top branch of the circuit represents the *I*

40

channel, and it is exactly the same as the single channel frequency converter. Similarly, the output signal from the bandpass filter is mixed with a locally generated sinusoid, $c(t)$, to give

$$y_I(t) = r'(t) \times c(t) = r'(t) \times A_c \cos(2\pi f_c t) \tag{41}$$
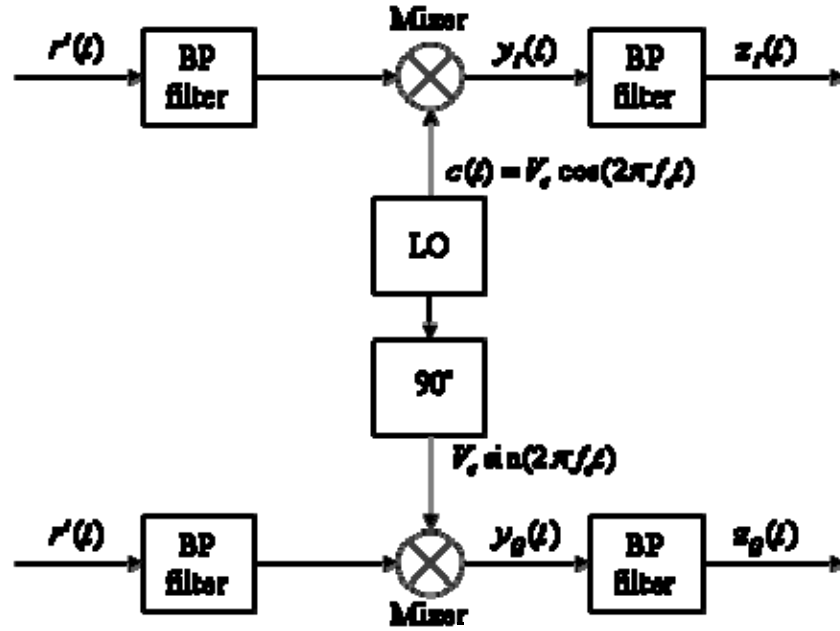
Figure 26.   In-Phase (I) and Quad-Phase (Q) Channel Frequency Down-Converter Circuit.

In the lower branch of the circuit, which represents the Q channel, the same sinusoid, $c(t)$, is shifted by 90° in phase to form $c\left(t - \frac{\pi}{2}\right) = V_c \cos\left(2\pi f_c t - \frac{\pi}{2}\right)$ $= V_c \sin(2\pi f_c t)$. The sinusoid is then mixed with the output signal from the bandpass filter to give

$$y_Q(t) = r'(t) \times c\left(t - \frac{\pi}{2}\right) = r'(t) \times A_c \sin(2\pi f_c t) \tag{42}$$

Both $y_I(t)$ and $y_Q(t)$ are passed through lowpass filters of critical frequency equals to $f_s/2$, so as to eliminate noise outside the frequency band of interest. The

outputs of the lowpass filters, $z_I(t)$ and $z_Q(t)$, are sampled to form the digitized signals, z_I and z_Q respectively. The two sampled data sequences are combined to form a complex data sequence as

$$z = z_I + jz_Q \qquad (43)$$

The FFT is performed on the complex data sequence, z, and the power spectrum generated is plotted in Figure 27. A distinct difference between the single and I and Q channel conversion is that the latter generated a spectrum with negative frequencies. The frequencies detected are -21.1 MHz, 8.6 MHz, 10.2 MHz, 29.7 MHz, and 39.1 MHz. As the spectrum is lowered by 2.4 GHz through mixing, the actual frequencies detected are 2.3789 GHz, 2.4086 GHz, 2.4102 GHz, 2.4297 GHz, and 2.4391 GHz. Unlike the single channel conversion that resulted in false detection at 2.2 GHz, the frequency 2.38 GHz in the received signal is detected correctly as 2.3789 GHz with 1.1 MHz error. This shows for the same ADC operating at maximum sampling rate, the bandwidth of interest is doubled with the use of I and Q channel conversion. The bandwidth of interest is thus equals to the sampling rate, f_s.
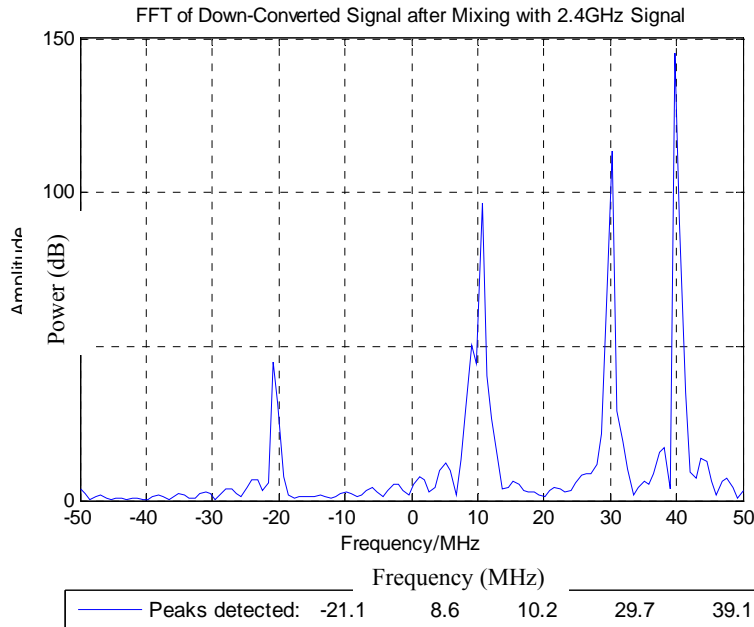
Figure 27.   Spectrum of Complex Data Sequence from I and Q Channel Frequency Down-Conversion.

G. SUMMARY

Before spectrum estimation is performed, the received analog signal has to be down-converted to baseband frequency and digitized. Single channel or I and Q channel can be used for the frequency down-conversion. It has been demonstrated that a bandpass filter is required before the frequency down-converter so as to prevent false detection due to frequencies outside the band of interest. For the single channel converter, the frequency band of interest is equal to half the sampling frequency, that is, $f_s/2$. As compared to the one channel converter, the I and Q channel converter has twice the frequency band of interest, which is equal to the sampling frequency, f_s. The single channel converter provides a real data sequence, and the I and Q channel provides a complex data sequence.

The next chapter focuses on applying the three selected high resolution spectrum estimation methods from Chapter II to the output data sequence.

THIS PAGE INTENTIONALLY LEFT BLANK

IV.   SIMULATION AND RESULTS

The first section of this chapter identifies candidate solutions to the frequency estimation function. In Section B, the power spectrum of the test signal from Eq. (40) is generated using the MUSIC method. In Section C, additive white Gaussian noise (AWGN) is added to the test signals before the spectrum is again generated by the MUSIC. In Section D, the same test signal is simulated with the ESPRIT method. In Section E, the simulation is repeated after the test signal is added with AWGN. In Section F, the MRSS is used to generate the power spectrum of the test signal. In the last section, the simulation is repeated after the test signal is added with AWGN.

A.   INTRODUCTION

In Chapter II, a signal with multi-tone spectrum was generated and passed through a bandpass filter, frequency down-converter, and an analog-to-digital (ADC) converter. The output is a digitized signal in its baseband, so that high resolution spectrum estimation can be performed. The FFT was demonstrated to have low spectral resolution. In this chapter, the power spectrum of the digitized signal is estimated using the MUSIC, ESPRIT and MRSS methods. The performances of the methods will be measured and evaluated. Additive white Gaussian noise (AWGN) will be added to the signal to quantify the robustness of the methods against noise. As the MUSIC is able to process complex data sequence, the I and Q channel frequency down-conversion is used to provide a wider frequency band of interest. On the contrary, the ESPRIT and MRSS are designed to process real data sequence, the single channel frequency down-conversion is used.

B.   ANALYSIS WITH MUSIC

The MUSIC method is used to estimate the spectrum of the signal from Eq. (40). The I and Q channel frequency down-conversion is used so as to double the bandwidth of interest to $f_s = 100$ MHz. There are $M = 7$ frequencies in the signal, namely 2.380 GHz, 2.410 GHz, 2.411 GHz, 2.4300 GHz, 2.4305 GHz, 2.4400 GHz and 2.4401 GHz. The

number of frequencies, *M*, is assumed to have been estimated correctly using Eq. (9). It is highlighted in Chapter II that the MUSIC is highly dependent on the accuracy of the number of frequencies in the signal. At this point, the signal is assumed to be free of noise.

When the order of the filter, *p*, is set to the minimum at $2M + 1 = 2 \times 7 + 1 = 15$, the power spectrum of the signal is plotted in Figure 28. The plot is distorted and shows numerous peaks.
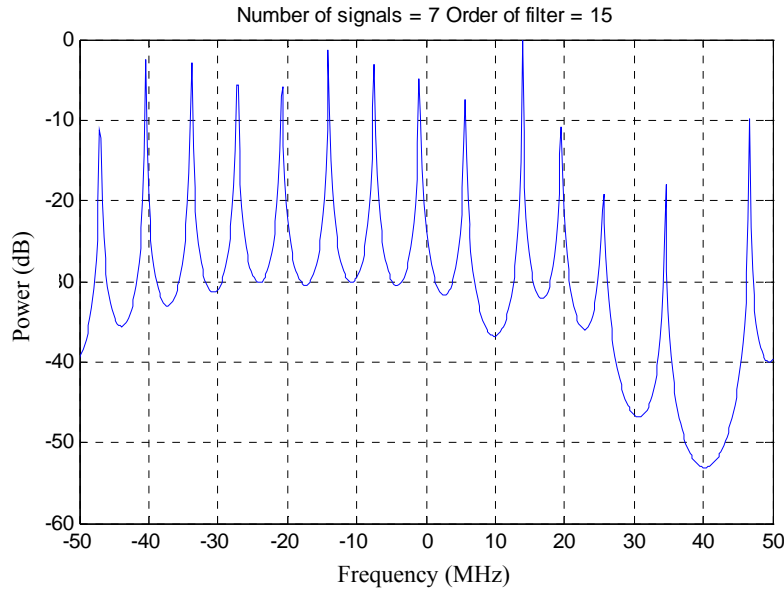
Figure 28.   Spectrum Using MUSIC for *M* = 7 and *p* = 15.

In Figure 29, *p* is incremented to 16, and five out of the seven frequencies in the received signal are detected. MUSIC is able to differentiate frequencies spaced at 0.5 MHz apart. Though there is a sharp peak at -20 MHz, the frequency may not be detected as the height of the peak is relatively low. The height of the peak is comparable to that of the broad peak at -50 MHz. The processing time is measured using the MATLAB function "tic" and "toc", and it includes the time required to identify the values of the peaks. The maximum estimation error is 0.1 MHz, and the processing time is 0.112968 s.

Number of signals = 7 Order of filter = 16

Peaks detected: 10   11   30.1   30.5   40.1

Figure 29.   Spectrum Using MUSIC for $M = 7$ and $p = 16$.

In Figure 30, p is incremented to 17. The spectrum is distorted and shows numerous peaks. The processing time is 0.115015 s.

Number of signals = 7 Order of filter = 17

Figure 30.   Spectrum Using MUSIC for $M = 7$ and $p = 17$.

As *p* increases to 18 and 19, the spectrum remains distorted. When *p* is increased to 20, the spectrum detects six out of seven frequencies in the received signal. The power spectrum for *p* equals to 20 is plotted in Figure 31. The MUSIC is still unable to differentiate the frequencies spaced at 0.1 MHz apart. The maximum estimation error is 0.1 MHz, and the processing time is 0.090337 s.
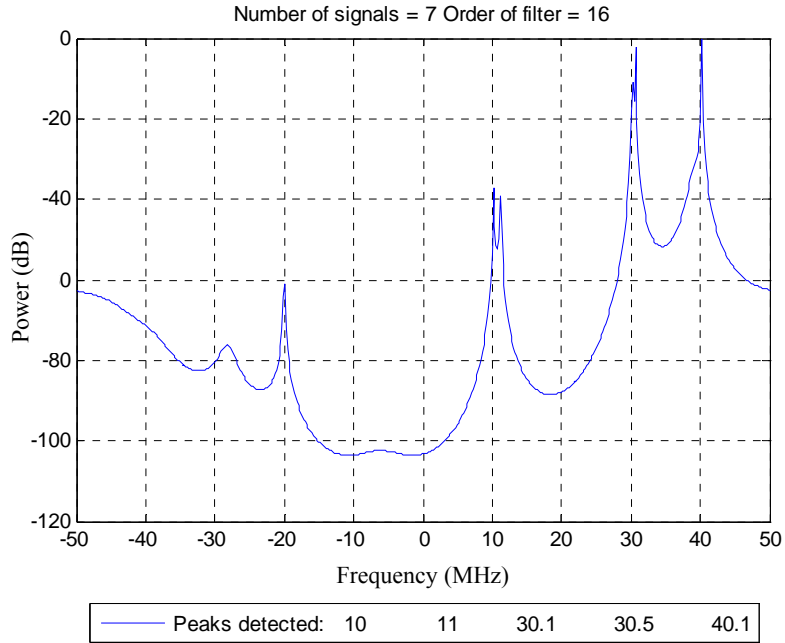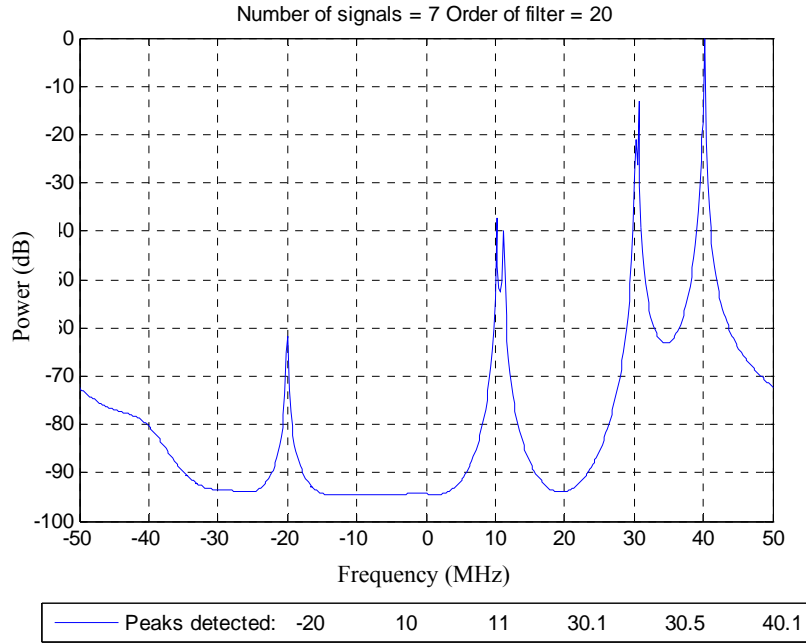

Figure 31.   Spectrum Using MUSIC for *M* = 7 and *p* = 20.

In Figure 32, *p* is incremented to 21. The spectrum is again distorted and shows numerous peaks. The processing time is 0.115015 s.
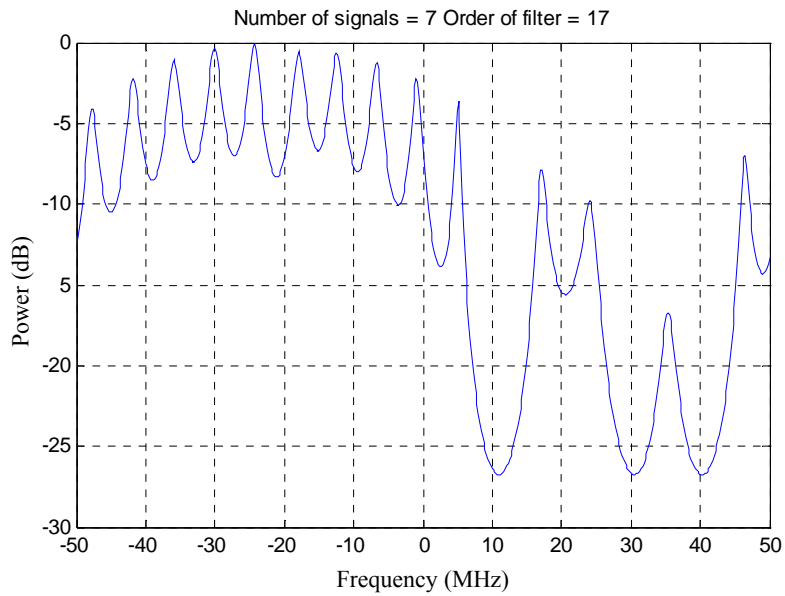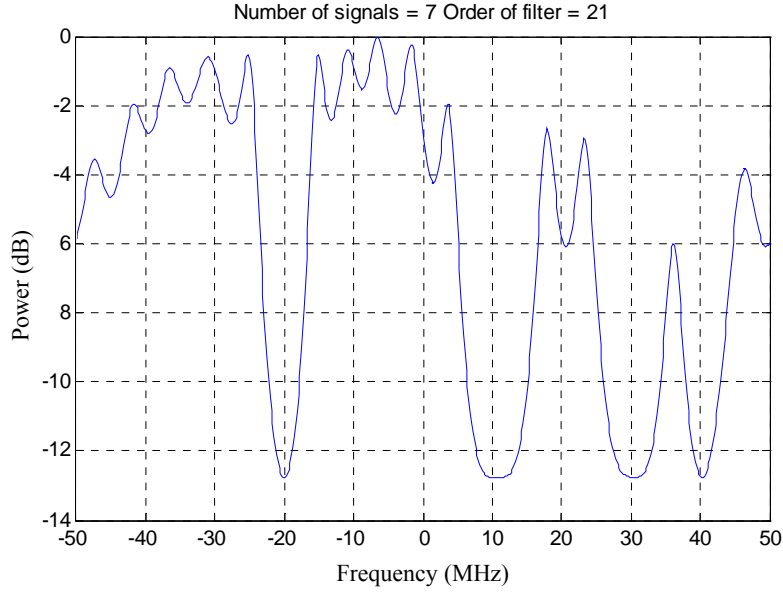
Figure 32.   Spectrum Using MUSIC for $M = 7$ and $p = 21$.

The above trend continues as p increases, and the spectrum is distorted for most values of p. As p increases, the spectrum will be distorted except when p equals to 24, 28, 32, 36, 40, 44, 48, …, or 92. This means that p has to be incremented by a value of four from 24 to generate non-distorted spectra. In Figure 33, p is incremented to 48, and the spectrum continues to show six out of the seven frequencies. The frequencies spaced at 0.5 MHz remains differentiable. The maximum estimation error is 0.1 MHz, and the processing time is 0.113248 s. It is observed that the heights of the peaks have reduced by about 10 dB as p increases from 24 to 48. The floor of the spectrum also increases by 10 dB from -85 dB to -75 dB. In Figure 34, the spectrum is distorted for p equal to 49.
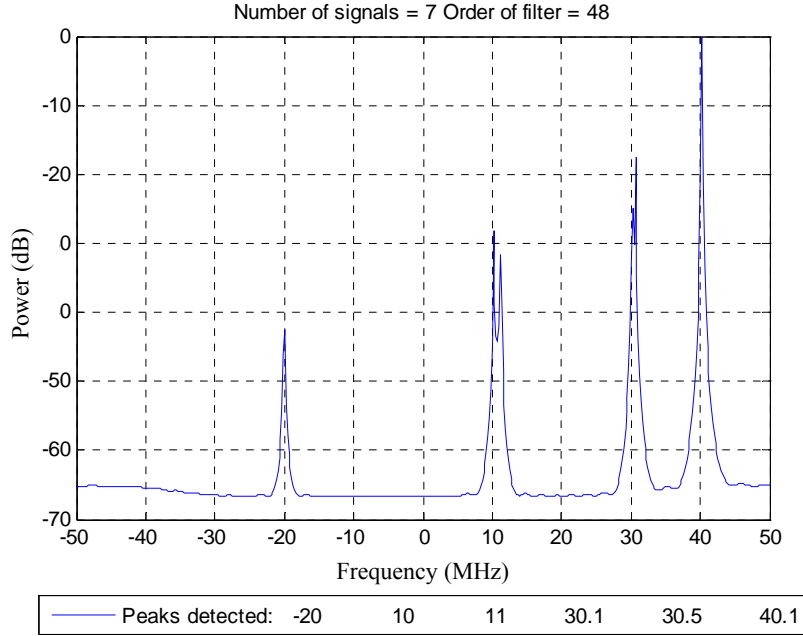
Figure 33.   Spectrum Using MUSIC for *M* = 7 and *p* = 48.
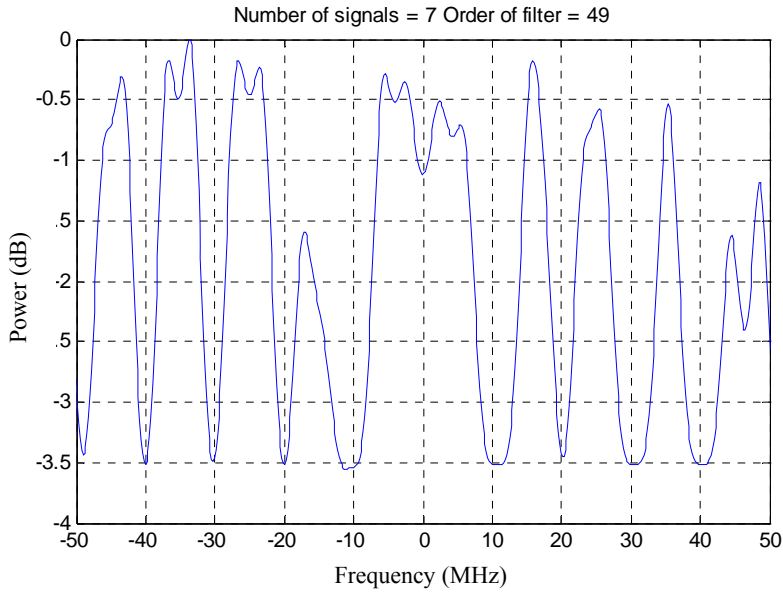
Figure 34.   Spectrum Using MUSIC for *M* = 7 and *p* = 49.

The recommended value of *p* is 2 *N* / 3 = 67.3 [4]. However, the spectrum is distorted when *p* equals to 67, but when *p* is rounded up to 68, the spectrum is plotted in Figure 35. Similarly, the spectrum shows six out of the seven frequencies, and it retains its ability to differentiate frequencies spaced at 0.5 MHz apart. The maximum estimation

error remains at 0.1 MHz, and the processing time is 0.116560 s. However, the floor of the spectrum increases by 9 dB from -65 dB to -56 dB, and the average height of the peaks reduces by about 5 dB.
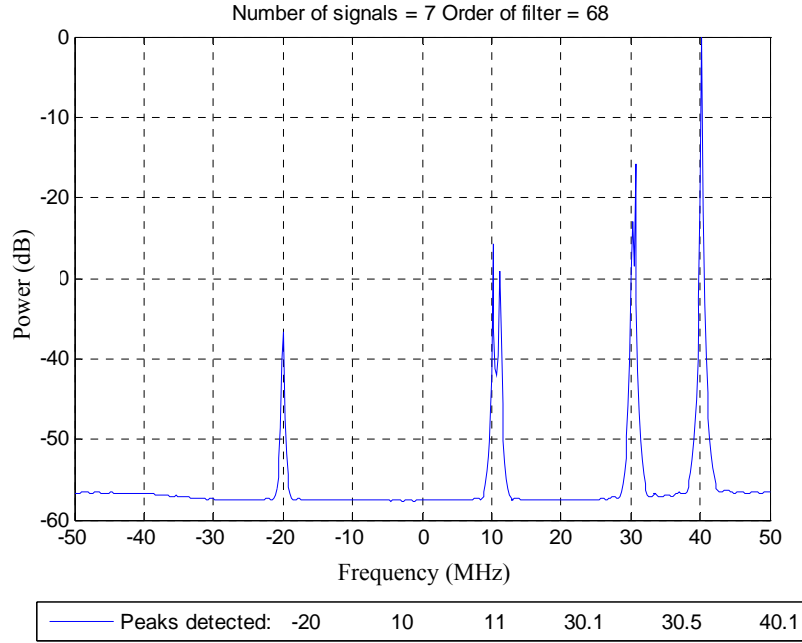
Figure 35.   Spectrum Using MUSIC for $M = 7$ and $p = 2 \, N / 3 \approx 68$.

In Figure 36, p is increased to 92. Similarly, the spectrum shows six out of the seven frequencies, and it retains its ability to differentiate frequencies spaced at 0.5 MHz apart. The maximum estimation error remains at 0.1 MHz, and the processing time is 0.132163 s. However, the floor of the spectrum increases by 23 dB from -56 dB to -33 dB, and the average height of the peaks reduces by about 3 dB.
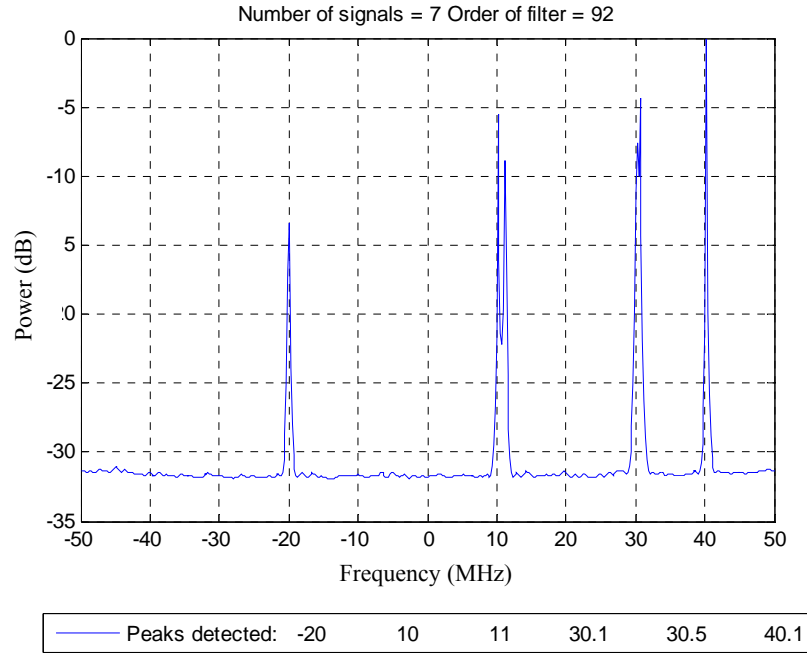
Figure 36.   Spectrum Using MUSIC for $M = 7$ and $p = 92$.

The highest value of p that the spectrum is not distorted is 101, which is an increment of 9 from 92. The spectrum is shown in Figure 37, and it detects only the two frequencies with the highest peaks. The maximum estimation error is 0.2 MHz, and the processing time is 0.143407 s. For p equals to or greater than 102, the spectrum is distorted.
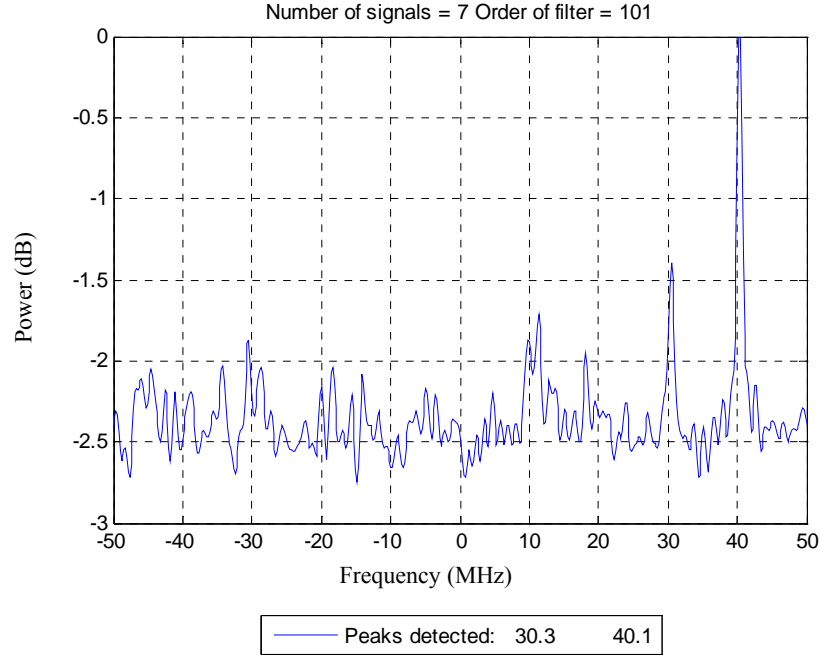
Figure 37.   Spectrum Using MUSIC for $M = 7$ and $p = 101$.

C.   ANALYSIS WITH MUSIC IN THE PRESENCE OF NOISE

To test the robustness of the MUSIC method in a noisy environment, the received signal, $r'(t)$, is added with additive white Gaussian noise (AWGN) such that the signal-to-noise ratio (SNR) is 10 dB. That is, the signal power is ten times that of the noise power. The performance of the MUSIC method is expected to deteriorate in the presence of noise.

As a comparison, the spectrum produced using the FFT is plotted in Figure 38. The spectrum is similar to the FFT of the noiseless signal shown in Figure 27.
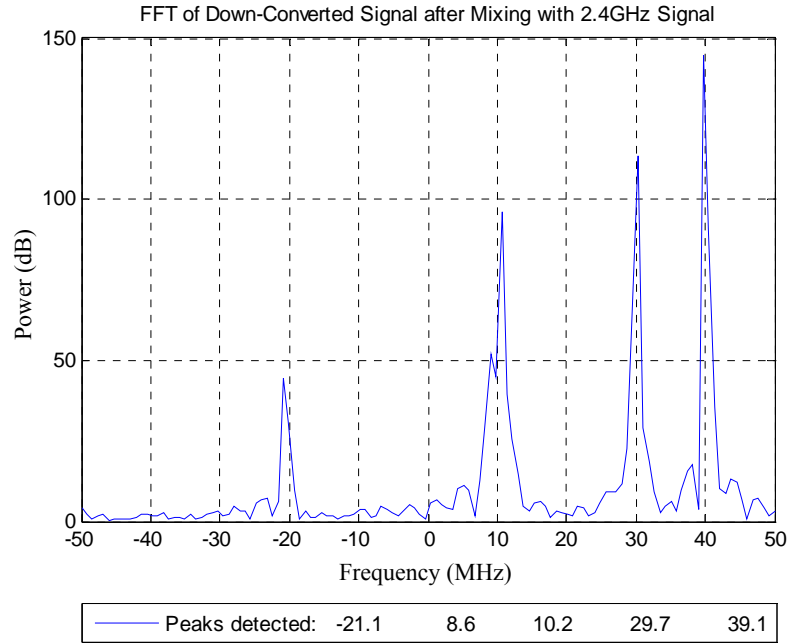
Figure 38. Spectrum Using FFT for SNR = 10 dB.

When the order of the filter, p, is set to the minimum at $2\,M + 1 = 2 \times 7 + 1 = 15$, the spectrum of the signal is plotted in Figure 39. The spectrum is distorted with numerous peaks. The processing time is 0.109423 s. Unlike the noiseless case, the spectrum remains distorted until p is increased to 24. This means that the minimum value of p for spectrum estimation increases in the presence of noise.
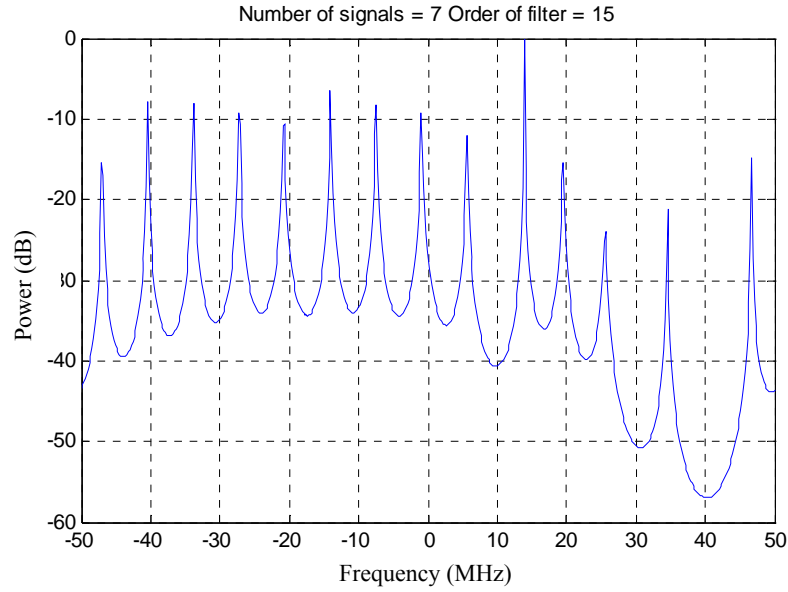
Figure 39.   Spectrum Using MUSIC for $M = 7$, $p = 15$, and SNR = 10 dB.

In Figure 40, p is increased to 24, and the spectrum detects five out of the seven frequencies. Unlike the noiseless case, the MUSIC loses its ability to differentiate frequencies spaced at 0.5 MHz apart. The maximum estimation error is 0.2 MHz, and the processing time is 0.085496 s. The three low-lying peaks may result in false detections if the threshold is not set properly.

Figure 40.　　　Spectrum Using MUSIC for $M = 7$, $p = 24$, and SNR = 10 dB.

The next value of p that the spectrum is not distorted is 28. The spectrum for p equals to 28 is generated in Figure 41. The MUSIC regains its ability to differentiate frequencies spaced at 0.5 MHz apart. The maximum estimation error is 0.1 MHz, and the processing time is 0.086582 s. The next value of p that the spectrum is not distorted is 32. In Figure 42, p equals to 32, and the characteristics of the spectrum remain unchanged. The maximum estimation error is 0.1 MHz, and the processing time is 0.092939 s.

Number of signals = 7 Order of filter = 28

Peaks detected: -20   10   11   30.1   30.5   40.1

Figure 41.   Spectrum Using MUSIC for $M = 7$, $p = 28$, and SNR = 10 dB.

Number of signals = 7 Order of filter = 32

Peaks detected: -20   10   11   30.1   30.5   40.1
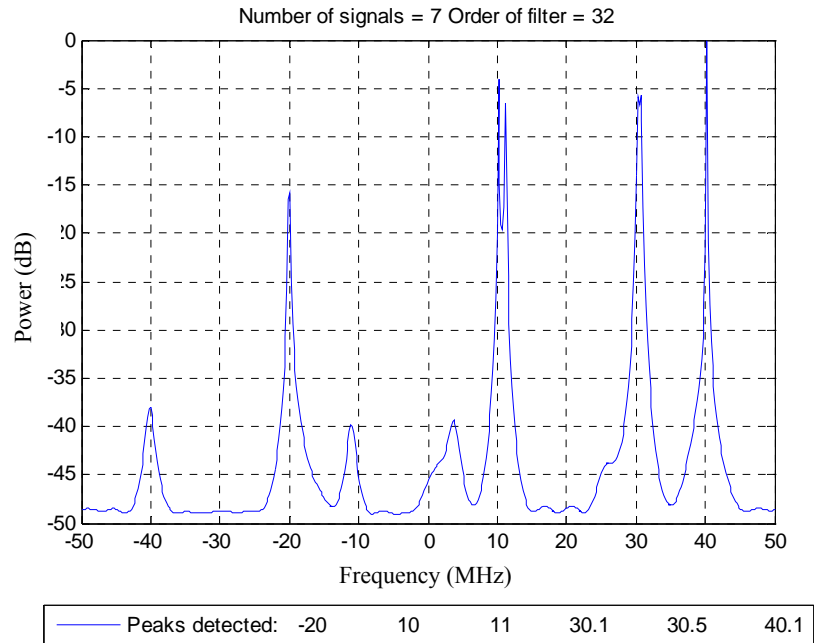
Figure 42.   Spectrum Using MUSIC for $M = 7$, $p = 32$, and SNR = 10 dB.

Figure 43 shows that the MUSIC again loses its ability to distinguish the pair of frequencies spaced at 0.5 MHz apart when p is incremented by 4 to 36. The maximum estimation error is 0.2 MHz, and the processing time is 0.089697 s. This shows that in the presence of noise, the order of the filter, p, must be equal to 28 or 32 so as to provide a spectral resolution of 0.5 MHz.
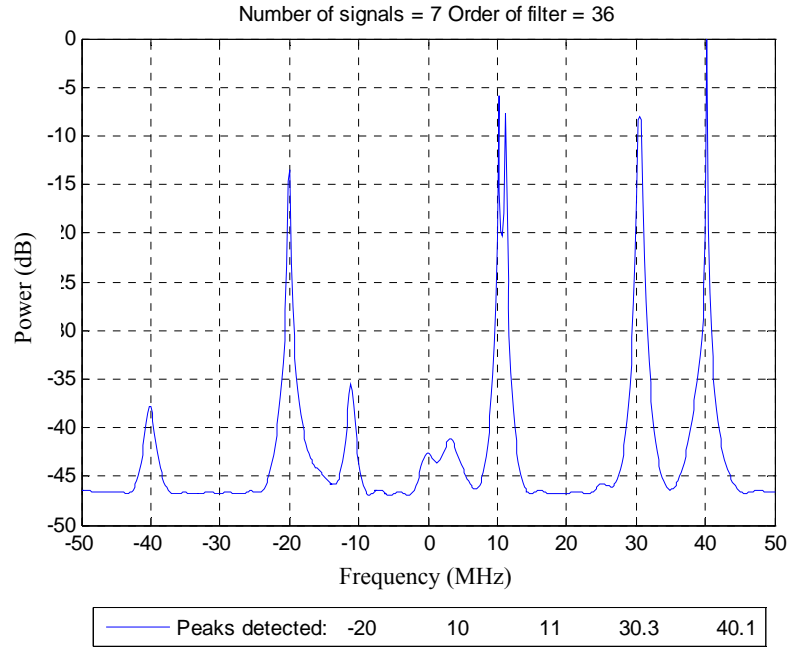
Figure 43.   Spectrum Using MUSIC for $M = 6$, $p = 34$, and SNR = 10 dB.

In Figure 44, the MUSIC is still able to distinguish the pair of frequencies spaced at 1 MHz apart when p is increases to 92. The maximum estimation error is 0.2 MHz, and the processing time is 0.119846 s.

Number of signals = 7 Order of filter = 92
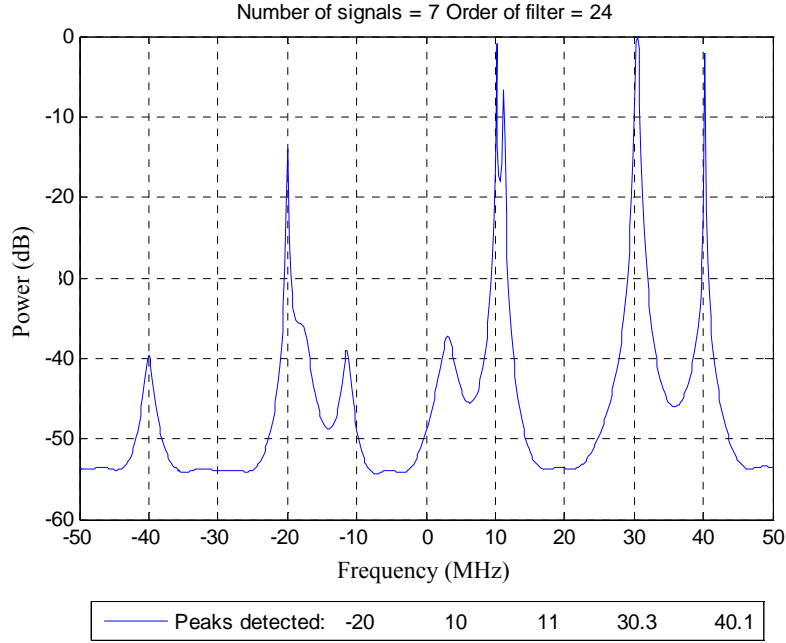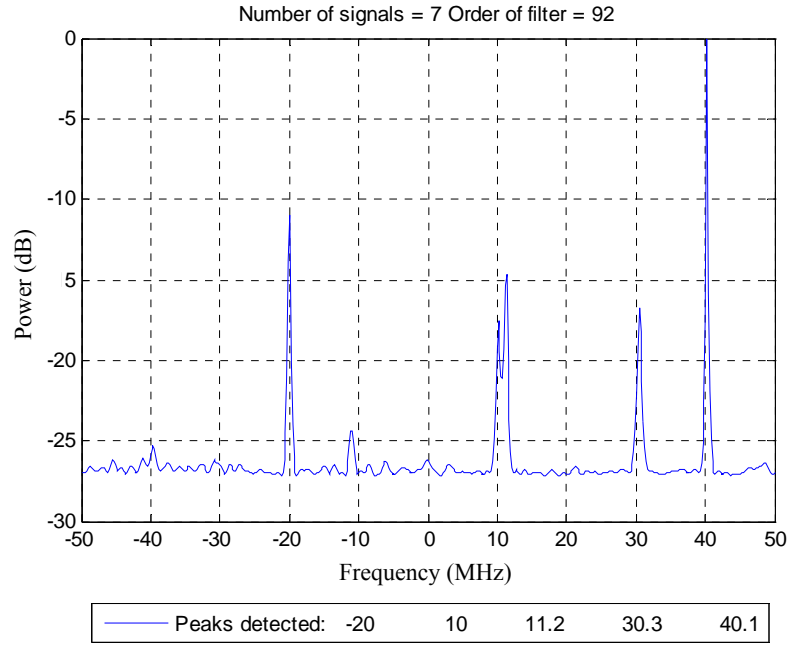

Figure 44.　　　Spectrum Using MUSIC for $M = 7$, $p = 92$, and SNR = 10 dB.

The last value of p that the spectrum is not distorted is 101, which is an increment of 9 from 92. The spectrum is shown in Figure 45, and it detects only the two frequencies with the highest peaks. The maximum estimation error is 0.2 MHz, and the processing time is 0.131457 s. For p equals to or greater than 102, the spectrum is distorted.
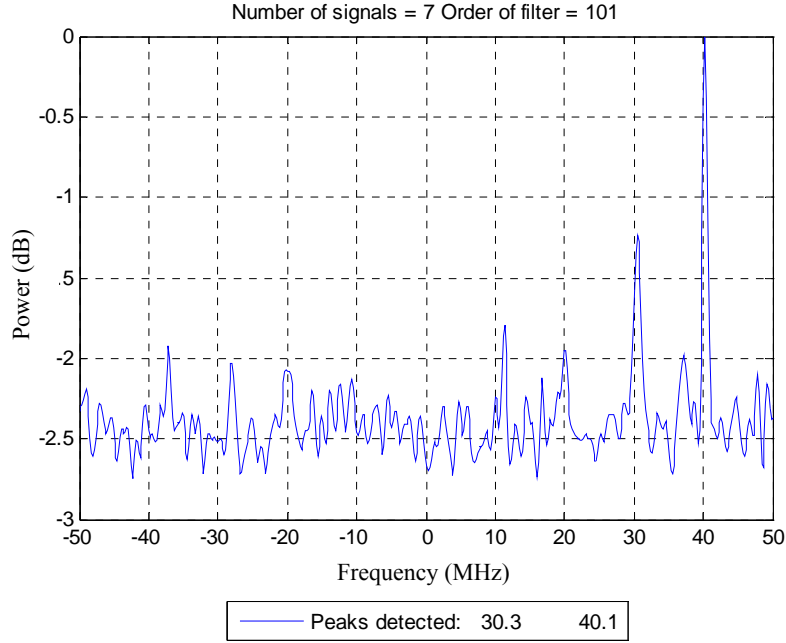
Figure 45.   Spectrum Using MUSIC for $M = 6$, $p = 50$, and SNR $= 10$ dB.

For SNR lower than 10 dB, the MUSIC loses its ability to differentiate frequencies spaced at 0.5 MHz apart for all values of p. This shows that the frequency resolution of MUSIC is not robust against the presence of noise in the received signal. In Figure 46 and Figure 47, the SNR is reduced to 9 dB and the order of filter, p, is set to 28 and 32 respectively. The frequencies spaced to 0.5 MHz can no longer be differentiated. However, the maximum estimation error is reduced to zero. The processing times are 0.094282 s and 0.094040 s, respectively.
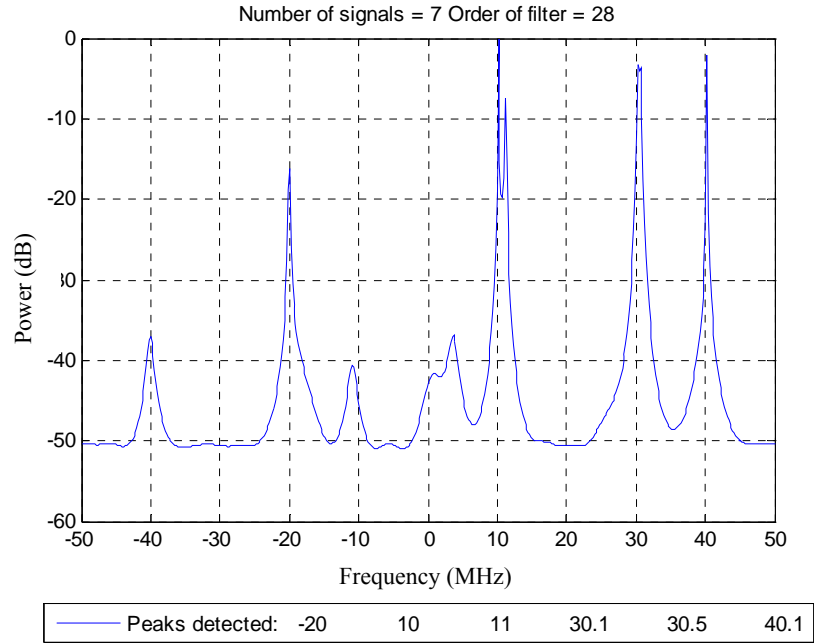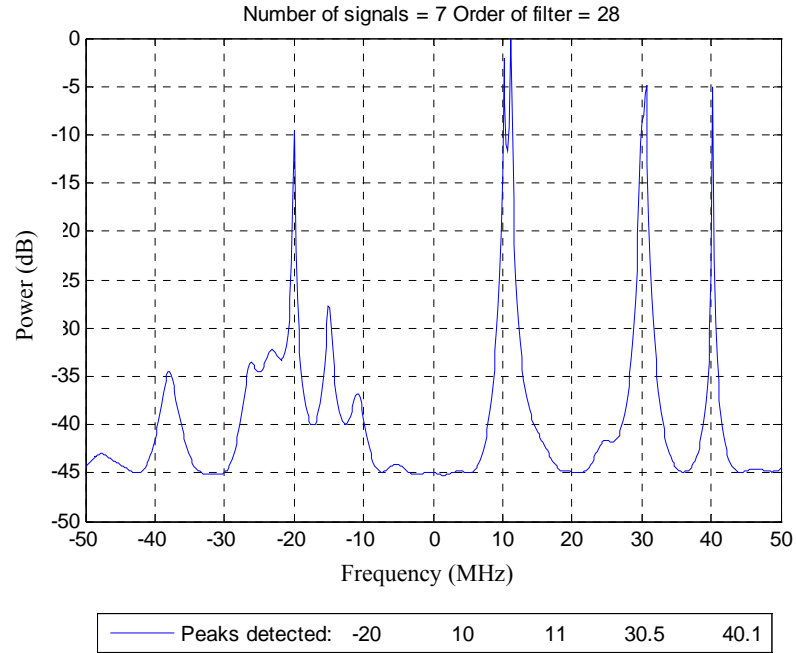
Figure 46.   Spectrum Using MUSIC for $M = 7$, $p = 28$, and SNR = 9 dB.
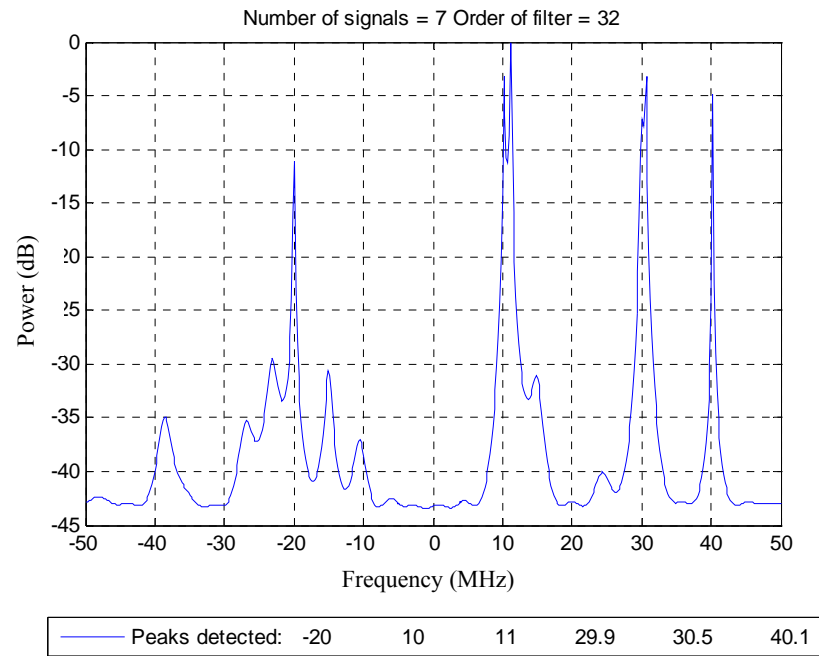
Figure 47.   Spectrum Using MUSIC for $M = 7$, $p = 32$, and SNR = 9 dB.

D.   ANALYSIS WITH ESPRIT

The ESPRIT method is used to estimate the spectrum of the signal from Eq. (40). Unlike MUSIC, ESPRIT is not able to identify the negative frequencies from the I and Q channel complex data sequence. This is because the ESPRIT method will search for real λ values close to the unit circle from Eq. (18). That is, the 4.38 GHz will be falsely detected as 4.42 GHz. Thus, the single channel frequency down-conversion is used, and corresponding bandwidth of interest is $f_s / 2 = 50$ MHz. It is highlighted in Chapter II that the ESPRIT is even more dependent on the accuracy of the number of frequencies, M, in the signal than the MUSIC method. At this point, the signal is assumed to be free of noise.

As the sinusoid at 4.38 GHz will be filtered off in the single channel frequency conversion, there are $M = 6$ frequencies to be detected in the signal from Eq. (40). To measure the effects of the accuracy of M on the ESPRIT method, the number of frequencies in the signal is varied from one to ten. The results of the frequencies detected and frequencies that are falsely detected are tabulated in Table 2. It is observed that the ESPRIT is able to identify all the six frequencies in the signal when M is correctly set to six. The ESPRIT method is able to differentiate frequencies that are closely spaced at 0.1 MHz apart. Its spectral resolution surpasses that of the MUSIC at 0.5 MHz.

For a value of M below six, $(6 - M)$ frequencies will not be detected. For a value of M greater than six, $(M - 6)$ frequencies will be falsely detected. This is because the ESPRIT method will search for M λ values close to the unit circle from Eq. (18), thus resulting in M frequency detections.

Table 2.   Frequencies Detected Using ESPRIT for $M = 1, 2, \ldots, 10$.

Number of Frequencies, M	Frequencies detected / MHz	Actual Frequencies Not Detected / MHz	Frequencies Falsely Detected / MHz
1	11	10, 30, 30.5, 40, 40.1	-
2	10.001, 11	30, 30.5, 40, 40.1	-
3	10.0010, 11.0000, 30.4980	30, 40, 40.1	-
4	10.0010, 11.0000, 30.4980, 40.0660	30, 40	-
5	10.0010, 11.0000, 30.0010, 30.4980, 40.0660	40	-
6	10.0010, 11.0000, 30.0010, 30.4980, 39.7840, 40.0660	-	-
7	10.0010, 11.0000, 19.6600, 30.0010, 30.4980, 39.7840, 40.0660	-	19.6600
8	3.8650, 10.0010, 11.0000, 19.6600, 30.0010, 30.4980, 39.7840, 40.0660	-	3.8650, 19.6600
9	3.8650, 10.0010, 11.0000, 13.2710, 19.6600, 30.0010, 30.4980, 39.7840, 40.0660	-	3.8650, 13.2710, 19.6600,
10	3.8650, 10.0010, 11.0000, 13.2710, 19.6600, 30.0010, 30.4980, 33.5470, 39.7840, 40.0660	-	3.8650, 13.2710, 19.6600, 33.5470,

The corresponding maximum error of the detected frequencies from the actual frequencies is tabulated in Table 3. The MATLAB processing time is also recorded in Table 3. It is observed that the ESPRIT has a maximum detection error of 0.216 MHz from the actual frequency component of 40 MHz. This constitutes an error of 0.54 %. The processing time fluctuates minimally at about 0.013 s.

Table 3.   Maximum Errors and Processing Time Using ESPRIT for $M = 1, 2,…,10$.

Number of Frequencies, M	Frequencies detected / MHz	Maximum Error / MHz	Processing Time / s
1	11	0	0.013089
2	10.001, 11	0.001	0.012981
3	10.0010, 11.0000, 30.4980	0.002	0.014020
4	10.0010, 11.0000, 30.4980, 40.0660	0.034	0.012552
5	10.0010, 11.0000, 30.0010, 30.4980, 40.0660	0.034	0.012342
6	10.0010, 11.0000, 30.0010, 30.4980, 39.7840, 40.0660	0.216	0.013297
7	10.0010, 11.0000, 19.6600, 30.0010, 30.4980, 39.7840, 40.0660	0.216	0.012634
8	3.8650, 10.0010, 11.0000, 19.6600, 30.0010, 30.4980, 39.7840, 40.0660	0.216	0.012721
9	3.8650, 10.0010, 11.0000, 13.2710, 19.6600, 30.0010, 30.4980, 39.7840, 40.0660	0.216	0.012673
10	3.8650, 10.0010, 11.0000, 13.2710, 19.6600, 30.0010, 30.4980, 33.5470, 39.7840, 40.0660	0.216	0.012648

E.   ANALYSIS WITH ESPRIT IN THE PRESENCE OF NOISE

The signal from Eq. (40) is simulated to be received in a noisy environment by adding AWGN to the signal. The SNR is varied and the power spectrum is estimated using the ESPRIT method. The presence of noise is expected to degrade the performance of the ESPRIT method. To measure the effects of noise on the performance of the ESPRIT method, the value of M is assumed to be pre-determined correctly and input into the ESPRIT system. The results are tabulated in Table 4. Similar to Section C for the MUSIC method, the SNR is set to 10 dB initially. The ESPRIT method is only able to detect five of the six frequencies. It also detects a frequency falsely at 12.4950 MHz. The noise power is reduced with respect to the signal power, and the SNR is increased in steps of 5 dB to 30 dB. However, even as the SNR is increased to 30 dB, the ESPRIT method remains unable to detect all the six frequencies, and a frequency is falsely detected in place of the 40 MHz frequency.

Table 4.　Frequencies Detected Using ESPRIT for $M = 1, 2,…, 10$ in the Presence of Noise.

SNR	Frequencies detected / MHz	Actual Frequencies Not Detected / MHz	Frequencies Falsely Detected / MHz
10	9.9260, 11.0450, 12.4950, 29.2500, 31.5610, 40.0520	40	12.4950
15	10.0220, 10.9930, 30.0070, 30.4830, 36.1890, 40.0590	40	36.1890
20	9.9810, 11.0130, 30.0420, 30.5150, 35.2890, 40.0570	40	35.2890
25	9.9880, 11.0070, 25.2070, 30.0040, 30.4820, 40.0620	40	25.2070
30	10.0000, 10.9990, 24.5860, 30.0050, 30.4910, 40.0580	40	24.5860

As the SNR is increased, the maximum error of the detected frequencies from the actual frequencies decreased significantly from 1.061 MHz to 0.042 MHz. That is, the accuracy of the ESPRIT method increased with lesser noise. The processing time remains about constant at 0.013 s.

Table 5.　Maximum Errors and Processing Time Using ESPRIT for $M = 1, 2,…, 10$ in the Presence of Noise.

SNR	Frequencies detected / MHz	Maximum Error / MHz	Processing Time / s
10	9.9260, 11.0450, 12.4950, 29.2500, 31.5610, 40.0520	1.061	0.013671
15	10.0220, 10.9930, 30.0070, 30.4830, 36.1890, 40.0590	0.041	0.013439
20	9.9810, 11.0130, 30.0420, 30.5150, 35.2890, 40.0570	0.043	0.014302
25	9.9880, 11.0070, 25.2070, 30.0040, 30.4820, 40.0620	0.038	0.014107
30	10.0000, 10.9990, 24.5860, 30.0050, 30.4910, 40.0580	0.042	0.012422

F.　ANALYSIS USING MRSS

For the present application, the MRSS is performed using a digital receiver, thus the frequency spectrum of interest is limited to half of the ADC sampling rate of 100 MHz. With a relatively small spectrum of interest of 50 MHz, the fine sensing technique is suffice to provide quick spectrum estimation. The MRSS method is used to estimate

the spectrum of the signal from Eq. (40). From Figure 12, the MRSS circuit shows that a real received signal is required for processing. Therefore, a single channel frequency conversion is performed to provide a real data sequence, which is input into the MRSS system. At this point, the signal is assumed to be free of noise.

The signal is captured over an observation window, T_w, of 1 μs. The sweep frequency, f_{sweep}, is set to be 10 kHz, which is 1/10 of the smallest frequency spacing of 0.1 MHz in the signal. The spectrum of the signal is generated using MRSS, and is plotted in Figure 48. The MRSS method detects four out of the six frequencies. Frequencies that are spaced at 0.5 MHz or less cannot be differentiated. The maximum error is 0.8 MHz, and the processing time is 1.521157 s.
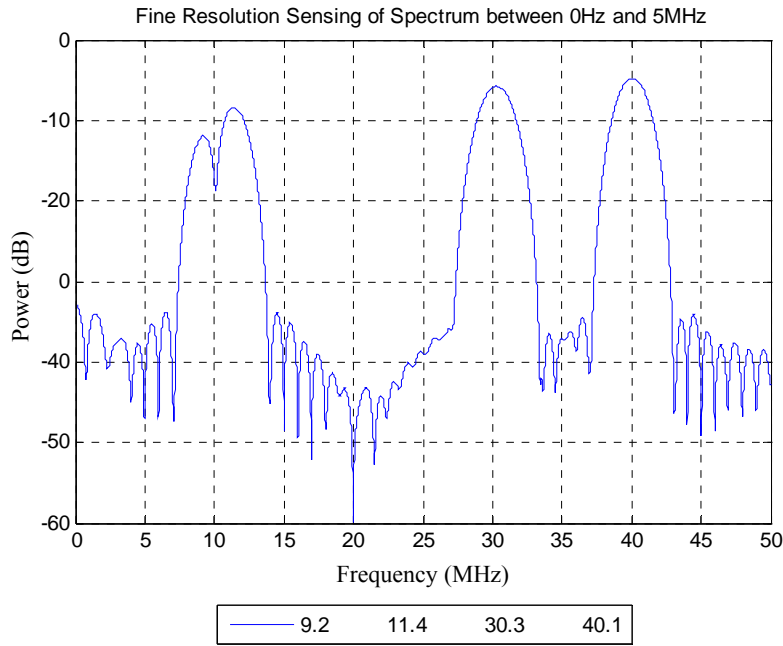

Figure 48.   Spectrum Using MRSS for T_w = 1 μs and f_{sweep} = 1 kHz.

It is demonstrated in Chapter II that the performance of the MRSS method is less dependent on the sweep frequency, f_{sweep}, and a value of f_{sweep} = 1/100 of frequency resolution required is sufficient. In Figure 49, the spectrum is generated for f_{sweep} = 1/100 of frequency resolution required = 1 kHz. The spectrum remains unchanged when f_{sweep} is reduced from 10 kHz to 1 kHz. The maximum estimation error remains unchanged at 0.8 MHz, but the processing time increases significantly from 1.521157 s to 27.328215 s.
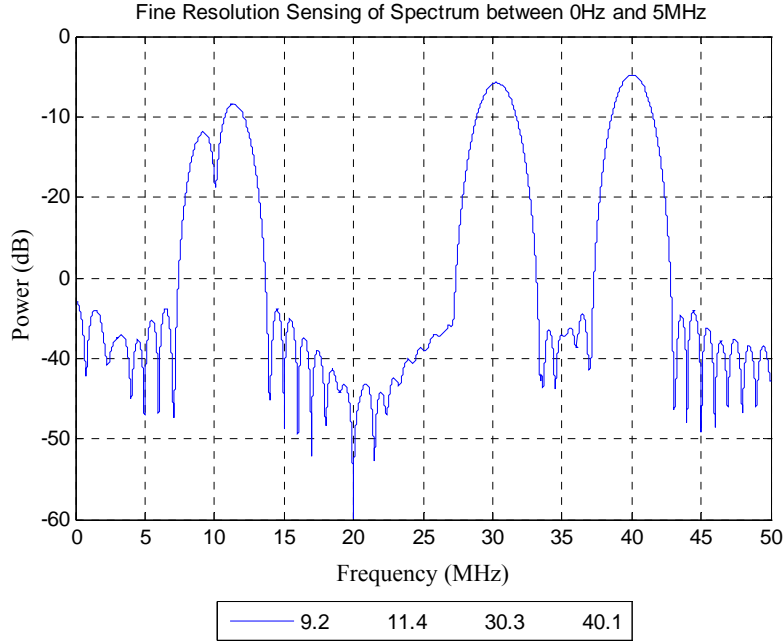
Figure 49.   Spectrum Using MRSS for $T_w = 1$ μs and $f_{sweep} = 1$ kHz.

In Figure 50, T_w is increased from 1 μs to 2 μs, and f_{sweep} is set to 10 kHz. The spectrum is not stable, as it loses its ability to differentiate the 1 MHz spaced frequencies. However, it is able to differentiate the frequencies spaced at 0.5 MHz apart. The maximum estimation error is 0.8 MHz, and the processing time is 1.574587 s. In Figure 51, when f_{sweep} is reduced to 1 kHz, the spectrum remains the same, but the processing time increases to 24.629242 s.

Figure 50. Spectrum Using MRSS for $T_w = 2$ μs and $f_{sweep} = 10$ kHz.
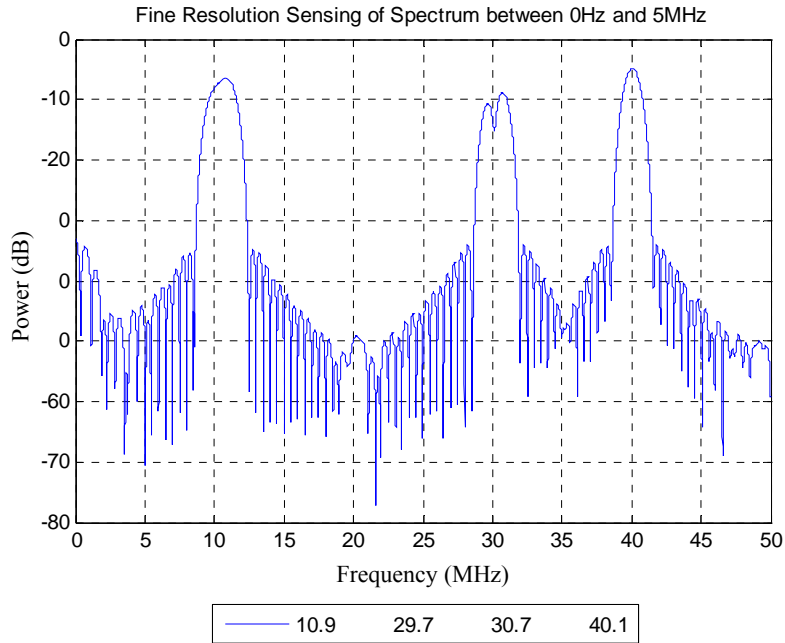
Figure 51. Spectrum Using MRSS for $T_w = 2$ μs and $f_{sweep} = 1$ kHz.

In Figure 52, T_w is increased to 3 μs, and f_{sweep} is set to 10 kHz. The spectrum stabilizes for T_w equals to or greater than 3 μs. The MRSS identifies four out of the six frequencies, and is able to differentiate the frequencies spaced at 1 MHz apart. The

68

maximum estimation error is reduced to zero, and the processing time is 1.568335 s. In Figure 53, when f_{sweep} is reduced to 1 kHz, the spectrum remains the same, but the processing time increases to 24.462193 s.
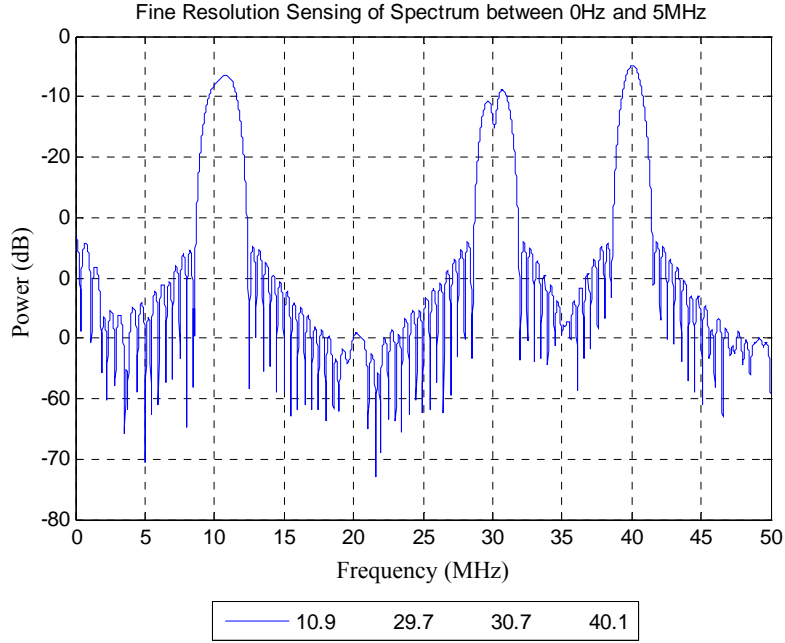

Figure 52.　　Spectrum Using MRSS for $T_w = 3$ μs and $f_{sweep} = 10$ kHz.

Figure 53.　　Spectrum Using MRSS Method for $T_w = 3$ μs, and $f_{sweep} = 1$ kHz.

In Figure 54, for f_{sweep} equals to 10 kHz, the MRSS is able to differentiate frequencies spaced at 0.5 MHz apart when T_w is increased to 5 μs. The five frequencies are estimated with zero error, and the processing time is 1.715302 s. In Figure 55, when f_{sweep} is reduced to 1 kHz, the spectrum remains the same, but the processing time increases to 16.625828 s.

Figure 54.　　Spectrum Using MRSS for $T_w = 5$ μs and $f_{sweep} = 1$ kHz.

Figure 55. Spectrum Using MRSS for $T_w = 5$ μs and $f_{sweep} = 1$ kHz.

In Figure 56, for f_{sweep} equals to 10 kHz, the MRSS is able to differentiate frequencies spaced at 0.1 MHz apart when T_w is increased to 9 μs. The six frequencies are estimated with zero error, and the processing time is 2.396204 s. It is observed that the peaks are more pronounced as T_w is increased. The floor of the signal reduces by about 10 dB from -58 dB to -68 dB. In Figure 57, when f_{sweep} is reduced to 1 kHz, the spectrum remains the same, but the processing time increases to 37.082383 s.
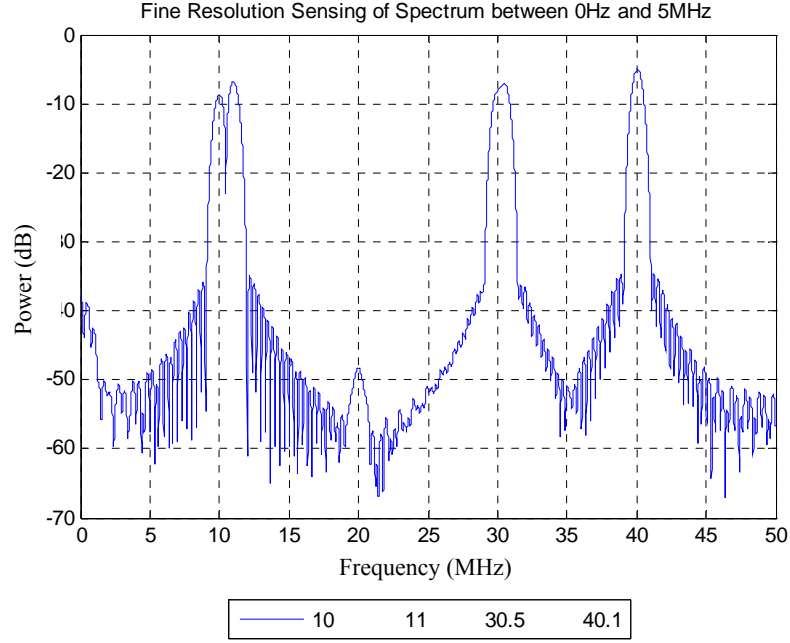
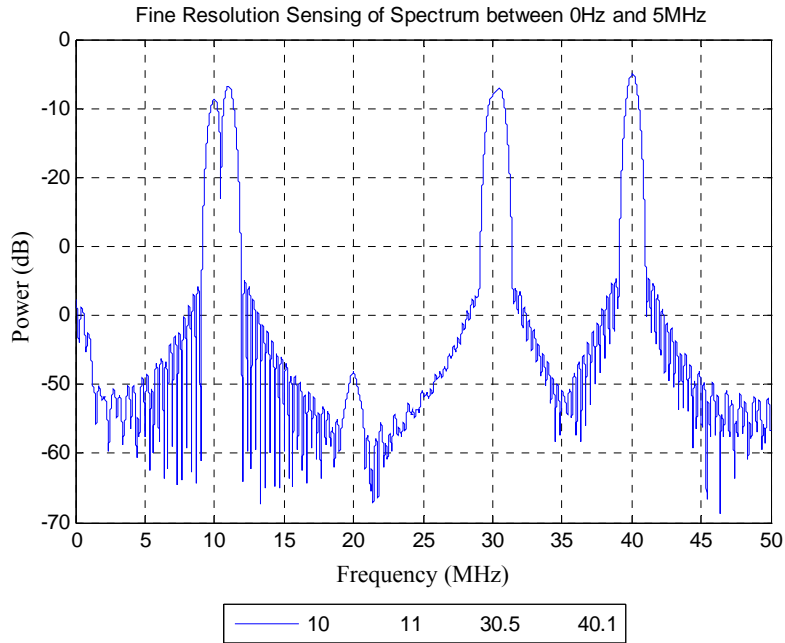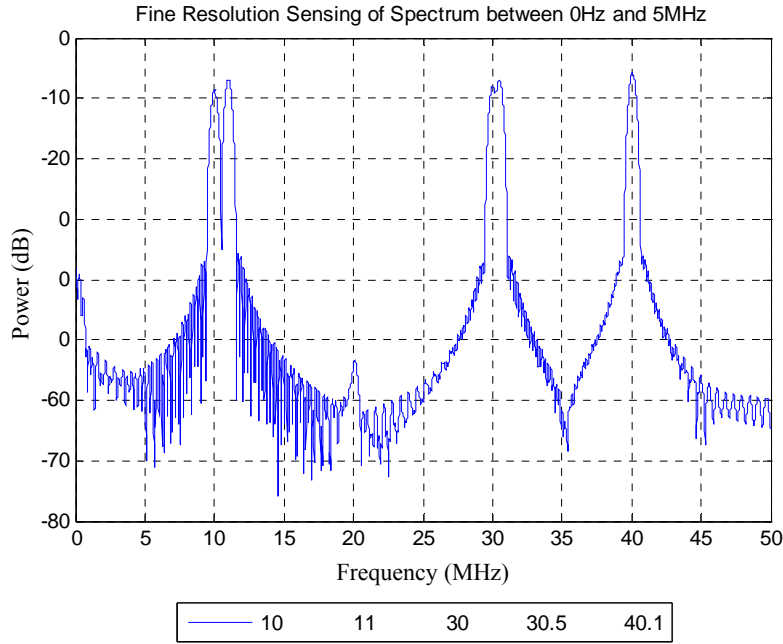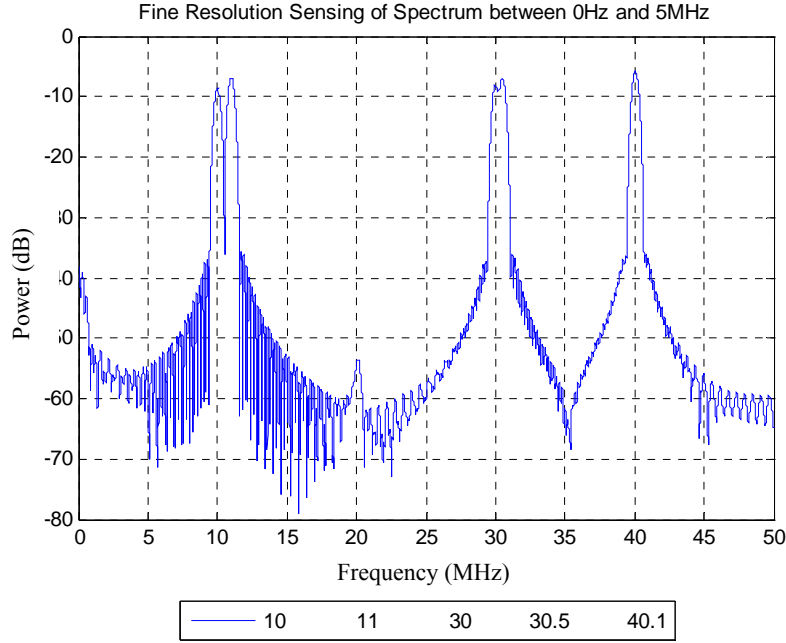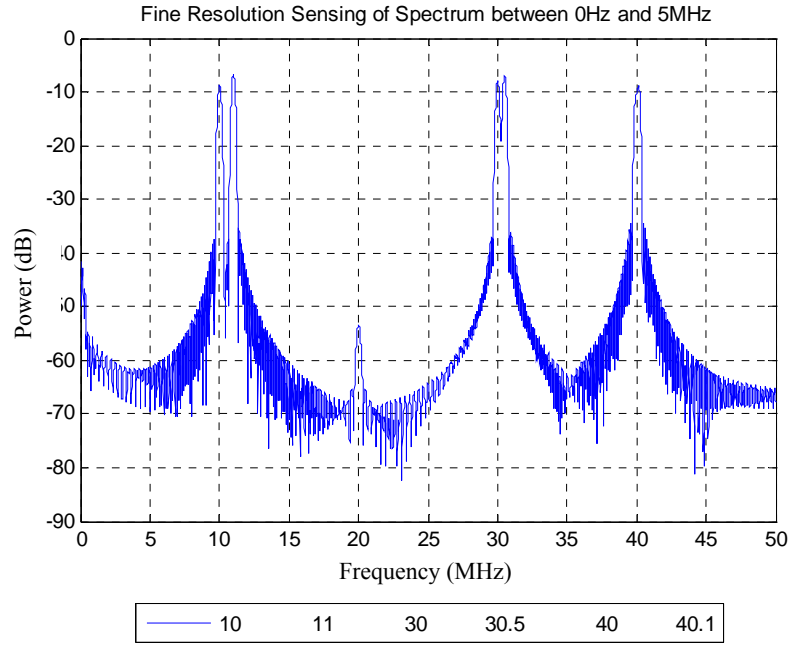Figure 56.   Spectrum Using MRSS for $T_w = 9$ μs and $f_{sweep} = 10$ kHz.
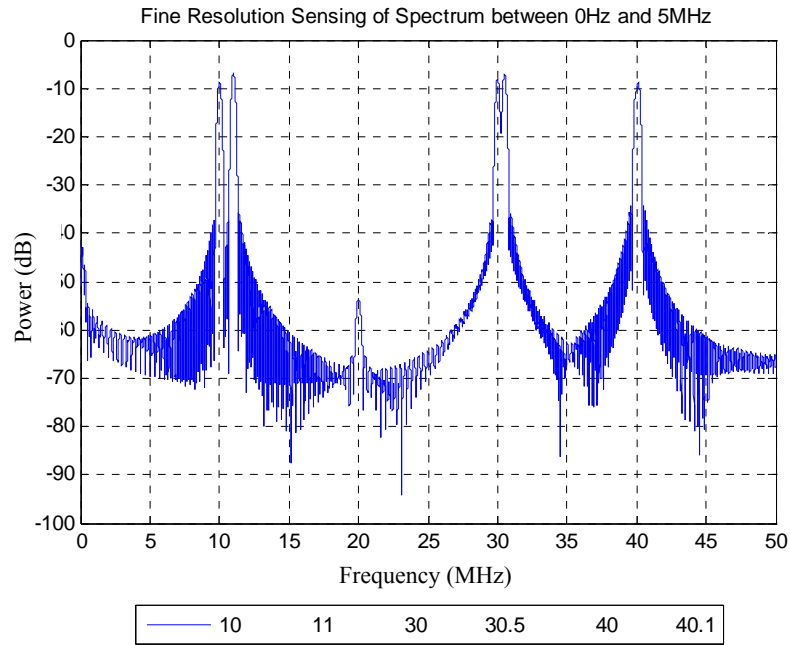
Figure 57.   Spectrum Using MRSS for $T_w = 9$ μs and $f_{sweep} = 1$ kHz.

G. ANALYSIS USING MRSS IN THE PRESENCE OF NOISE

The MRSS is simulated to analyze the signal from Eq. (40) in an AWGN environment. Similarly, the presence of noise is expected to degrade the performance of the MRSS method.

The noise power is first set to achieve a SNR of 10 dB. For T_w equals to 3 μs and f_{sweep} equals to 10 kHz, the spectrum generated by the MRSS is plotted in Figure 58. Similar to the noiseless case, the spectrum stabilizes for T_w equals or greater than 3 μs, and the frequencies spaced at 1 MHz can be differentiated. Though noise is introduced, the maximum error of frequency estimation remains at zero. The processing time is 1.670444 s. In Figure 59, f_{sweep} is reduced to 1 kHz, but the spectrum remains unchanged. The processing time is increased to 29.532189 s.

Figure 58.   Spectrum Using MRSS for $T_w = 3$ μs, $f_{sweep} = 10$ kHz, and SNR $= 10$ dB.
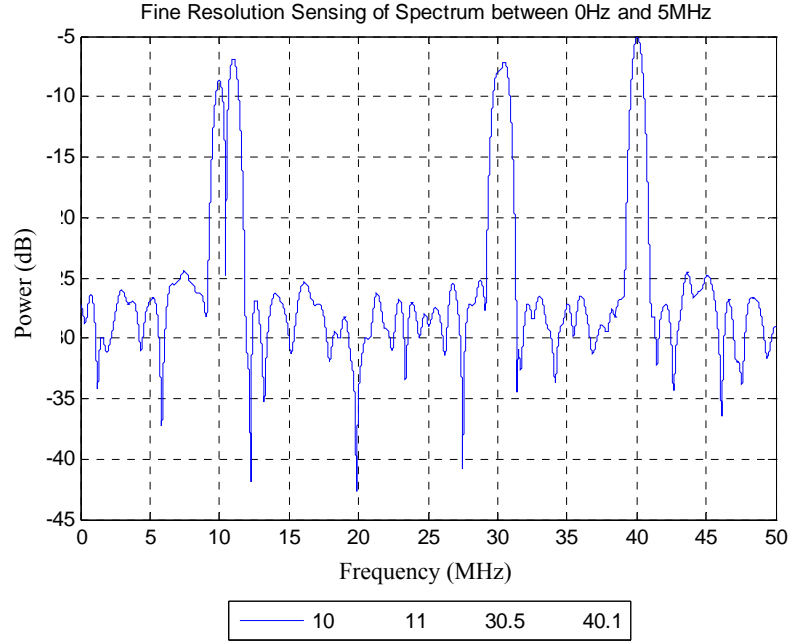
Figure 59.   Spectrum Using MRSS for $T_w = 3$ μs, $f_{sweep} = 1$ kHz, and SNR $= 10$ dB.

In Figure 60, T_w is increased to 5 μs. As in the noiseless case, the MRSS is able to differentiate the frequencies spaced at 0.5 MHz apart. The maximum frequency estimation error remains at zero. The processing time is 1.694698 s. In Figure 61, f_{sweep} is reduced to 1 kHz, but the spectrum remains unchanged. The processing time is increased to 28.674728 s.

Fine Resolution Sensing of Spectrum between 0Hz and 5MHz
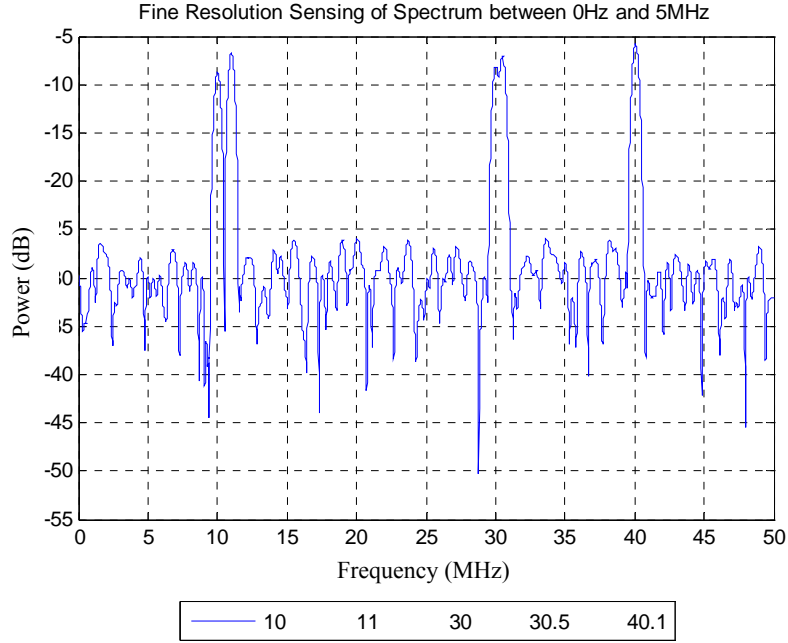
Figure 60.   Spectrum Using MRSS for $T_w = 5$ μs, $f_{sweep} = 10$ kHz, and SNR = 10 dB.

Fine Resolution Sensing of Spectrum between 0Hz and 5MHz
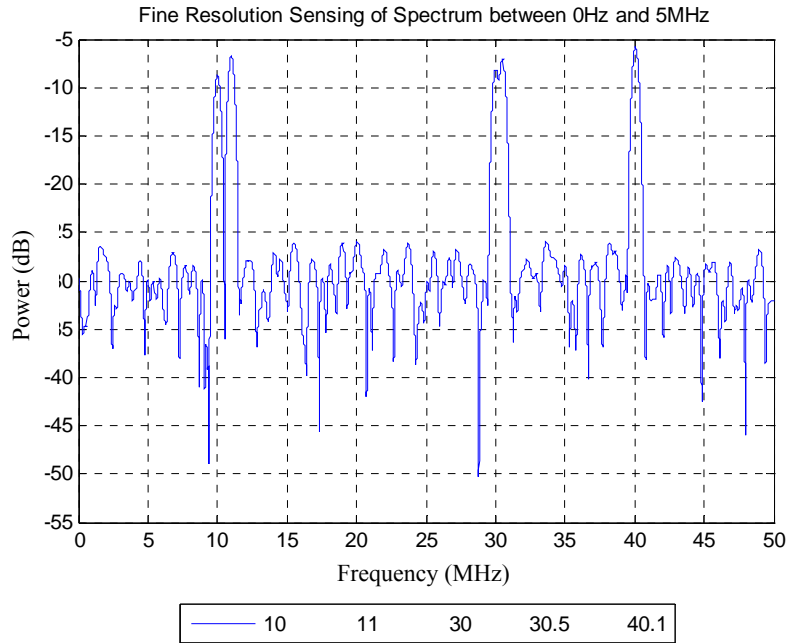
Figure 61.   Spectrum Using MRSS for $T_w = 5$ μs, $f_{sweep} = 1$ kHz, and SNR = 10 dB.

In Figure 62, T_w is increased to 9 μs. As in the noiseless case, the MRSS is able to differentiate the frequencies spaced at 0.1 MHz apart. The maximum frequency estimation error remains at zero. The processing time is 2.020169 s. In Figure 63, f_{sweep} is

75

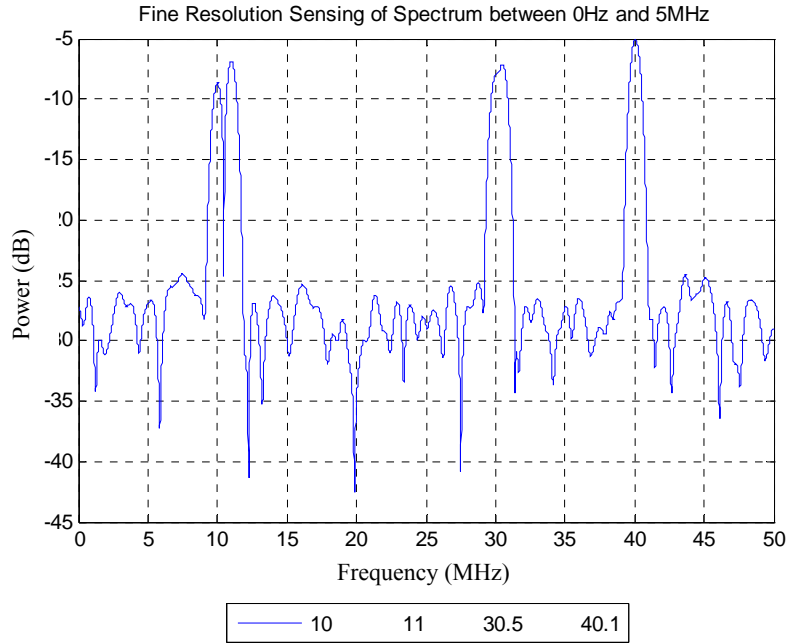reduced to 1 kHz, but the spectrum remains unchanged. The processing time is increased to 37.374430 s.

Fine Resolution Sensing of Spectrum between 0Hz and 5MHz
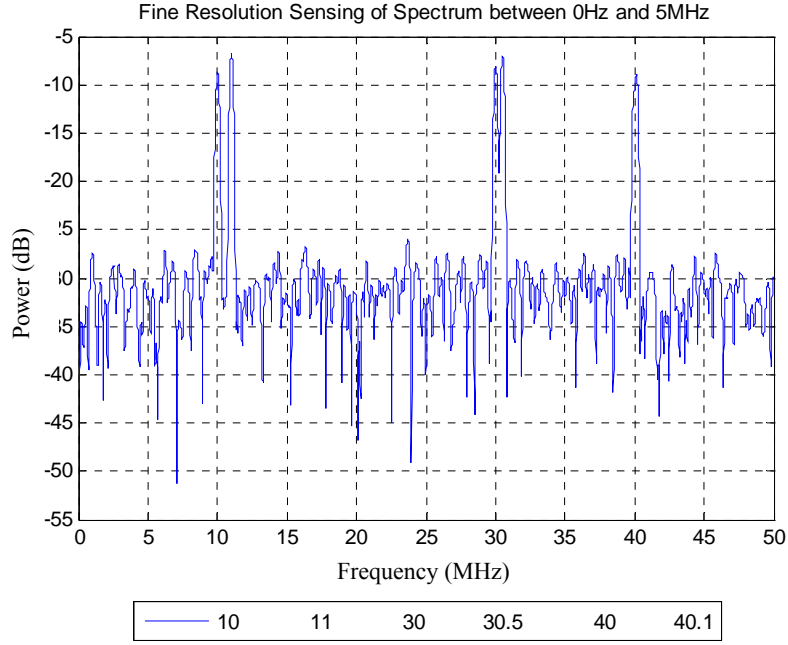
Figure 62.   Spectrum Using MRSS for $T_w = 9$ µs, $f_{sweep} = 10$ kHz, and SNR = 10 dB.

Fine Resolution Sensing of Spectrum between 0Hz and 5MHz
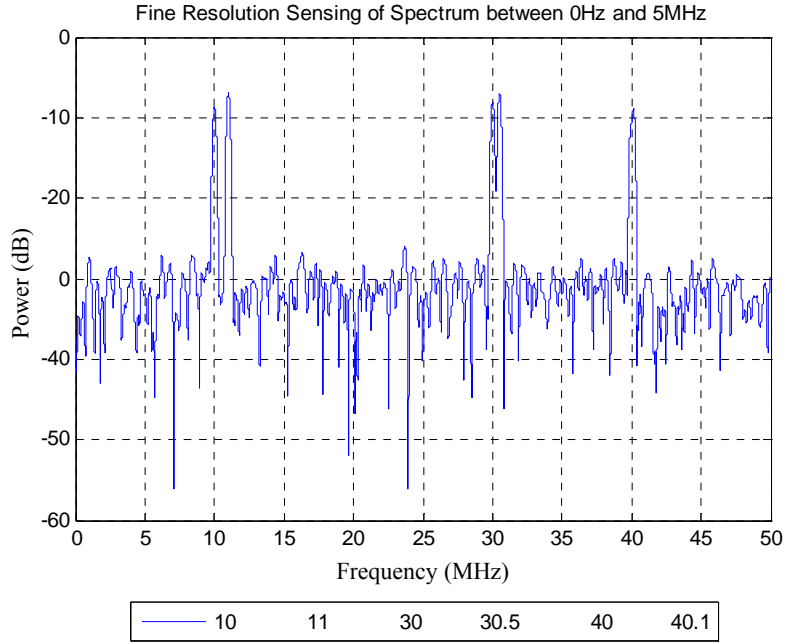
Figure 63.   Spectrum Using MRSS for $T_w = 9$ µs, $f_{sweep} = 1$ kHz, and SNR = 10 dB.

The frequency resolution and estimation accuracy of the MRSS is demonstrated to be robust in a noisy environment of 10 dB SNR. The SNR is further reduced to 0 dB, that is, the noise power is equal to the signal power. The value of f_{sweep} is set to 10 kHz, as it has been sufficiently demonstrated that 1/10 of the frequency resolution of the signal is suffice for accurate spectral estimation. It is also demonstrated that reducing f_{sweep} will not improve the frequency resolution, but it will increase the processing time significantly.

In Figure 64, T_w is set to 3 μs. As in the 10 dB SNR case, the MRSS is able to differentiate the frequencies spaced at 0.5 MHz apart. However, the heights of the peaks are reduced by about 7 dB from 22 dB to 15 dB. This is partly due to the increase in the floor of the signal by about 4 dB from -27 dB to -23 dB. The maximum frequency estimation error remains at zero, and the processing time is 1.615260 s.

Figure 64. Spectrum Using MRSS for T_w = 3 μs, f_{sweep} = 10 kHz, and SNR = 0 dB.

In Figure 65, T_w is increased to 5 μs. Similar to the 10 dB SNR case, the MRSS is able to differentiate the frequencies spaced at 0.5 MHz apart. The maximum frequency estimation error remains at zero, and the processing time is 1.752301 s.

Fine Resolution Sensing of Spectrum between 0Hz and 5MHz

Figure 65.   Spectrum Using MRSS 0 for $T_w = 5$ μs, $f_{sweep} = 10$ kHz, and SNR = 0 dB.

In Figure 66, T_w is increased to 9 μs. Similar to the 10 dB SNR case, the MRSS is able to differentiate the frequencies spaced at 0.1 MHz apart. The maximum frequency estimation error remains at zero, and the processing time is 1.986819 s.

Fine Resolution Sensing of Spectrum between 0Hz and 5MHz

Figure 66.   Spectrum Using MRSS for $T_w = 9$ μs, $f_{sweep} = 10$ kHz, and SNR = 0 dB.

78

The frequency resolution and estimation accuracy of the MRSS is demonstrated to be robust in a noisy environment of 0 dB SNR. The SNR is further reduced to -10 dB, that is, the noise power is ten times that of the signal power. In Figure 67, the T_w is set to be 3 μs. As in the 0 dB SNR case, the MRSS is able to differentiate the frequencies spaced at 0.5 MHz apart. However, the heights of the peaks are further reduced by about 5 dB from 15 dB to 12 dB. This is partly due to the increase in the floor of the signal of about 3 dB from -23 dB to -20 dB. The maximum frequency estimation error remains at zero, and the processing time is 1.527710 s.
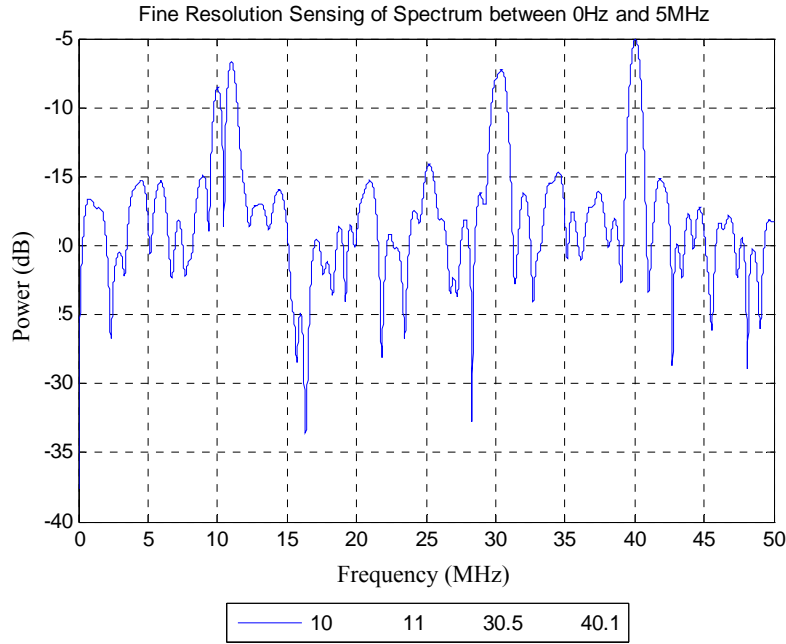
Figure 67.   Spectrum Using MRSS for $T_w = 3$ μs, $f_{sweep} = 10$ kHz, and SNR = -10 dB.

In Figure 68, T_w is increased to 5 μs. Similar to the 0 dB SNR case, the MRSS is able to differentiate the frequencies spaced at 0.5 MHz apart. The maximum frequency estimation error remains at zero, and the processing time is 1.642263 s.
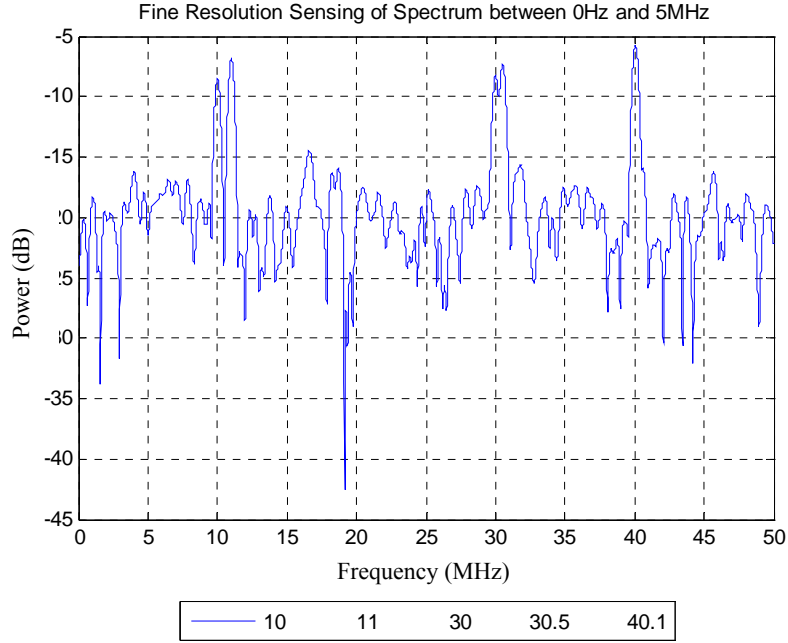
Figure 68. Spectrum Using MRSS for $T_w = 5$ μs, $f_{sweep} = 10$ kHz, and SNR = -10 dB.

In Figure 69, T_w is increased to 9 μs. Unlike the 0 dB SNR case, the MRSS is not able to differentiate the frequencies spaced at 0.1 MHz apart. The maximum frequency estimation error remains at zero, and the processing time is 2.050098 s.
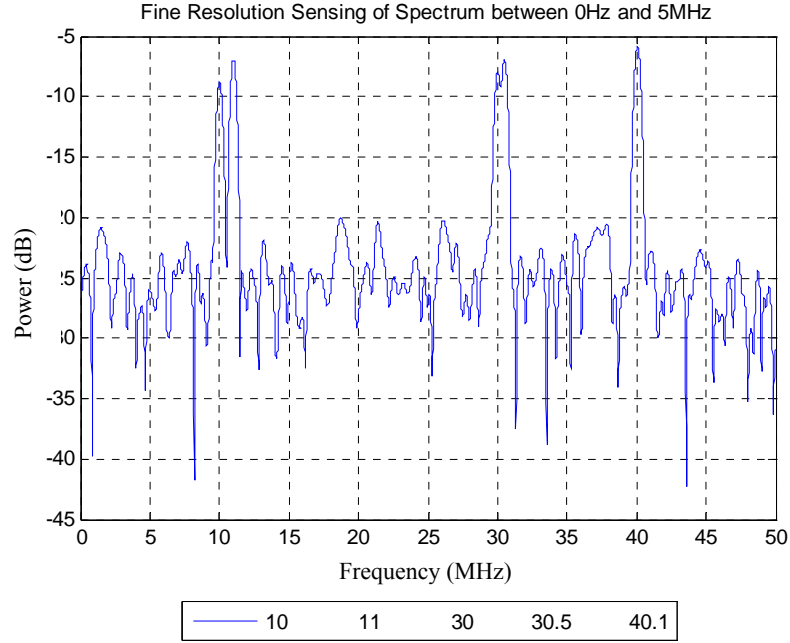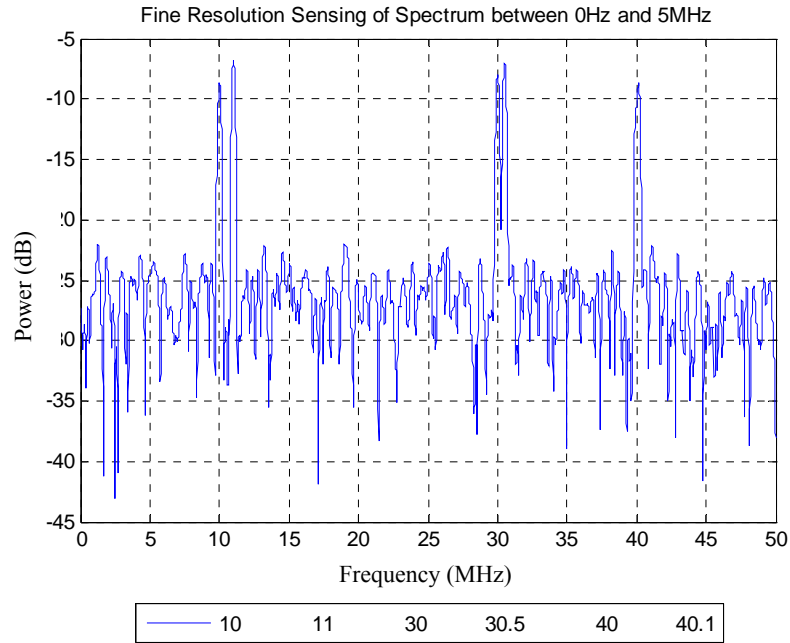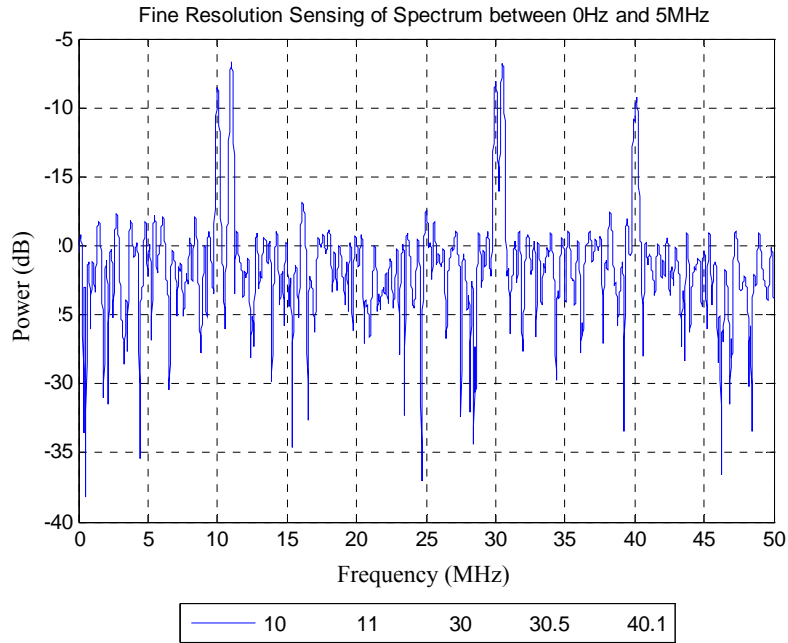

Figure 69. Spectrum Using MRSS for $T_w = 9$ μs, $f_{sweep} = 10$ kHz, and SNR = -10 dB.

In Figure 70, the MRSS regains its ability to differentiate the frequencies spaced at 0.1 MHz apart when T_w is increased by 4 μs to 13 μs. The maximum frequency estimation error remains at zero, and the processing time is 2.184246 s. This shows that the spectral resolution of the MRSS can be improved by increasing the observation time of the received signal. It also means that for a fixed spectral resolution, the observation time increases when the SNR decreases.
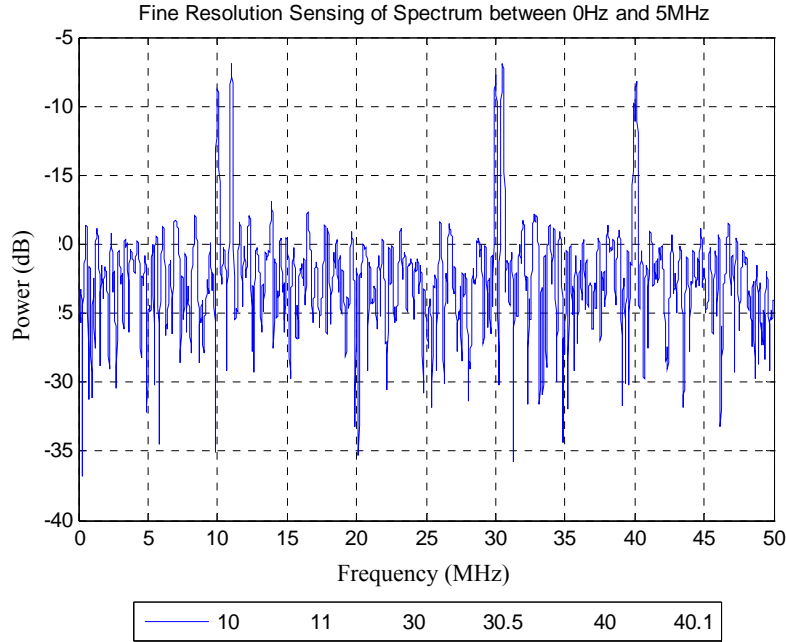
Figure 70.   Spectrum Using MRSS for $T_w = 13$ μs, $f_{sweep} = 10$ kHz, & SNR = -10 dB.

H.   SUMMARY

Before spectrum estimation is performed, the received analog signal is bandpassed, down-converted to baseband frequency, and digitized to produce a real or complex data sequence. As the MUSIC is able to process complex data sequence, the I and Q channel frequency down-conversion is used to provide a wider frequency band of interest at f_s. On the contrary, the ESPRIT and MRSS are designed to process real data sequence, thus the single channel frequency down-conversion is used to provide a frequency band of interest at $f_s/2$.

THIS PAGE INTENTIONALLY LEFT BLANK

V.   SUMMARY AND CONCLUSION

The first section of this chapter provides an overview of the frequency estimation module, and states the object of this chapter. In Section B, the simulations results from Chapter III are summarized and analyzed. In Section C, this thesis is concluded with a recommended high resolution spectrum estimation method for the digital tracking array.

A.   INTRODUCTION

In Chapter II, the test signal from Eq. (40) was bandpassed, down-converted to baseband frequency, and digitized. In Chapter III, the digital baseband signal was passed into the MUSIC, ESPRIT and MRSS to generate the power spectra. The results are consolidated and summarized in this chapter for efficient comparison. The performances and limitations of each high resolution spectrum estimation method are presented and compared between the three distinct methods. A high resolution spectrum estimation method will be recommended for the digital tracking array.

B.   SUMMARY OF SIMULATION RESULTS

The simulation results from Chapter III are summarized in Table 6. For the MUSIC, the smallest spectral resolution achievable is 0.5 MHz. However, to retain the 0.5 MHz spectral resolution, the SNR must be equal to or greater than 10 dB. It has a relatively small maximum estimation error of about 0.2 MHz in the 100 MHz spectrum of interest. The accuracy of the spectrum is dependent on the accuracy of the estimated number of frequencies, M, in the received signal. If M is over-estimated, false frequency detection will occur. If M is under-estimated, frequencies in the received signal will not be detected. For 0.5 MHz spectral resolution, when applied to seven signals, the order of the filter, p, can only take on discrete values from 20, 24, 28,…, 92 in increment of 4. The spectrum is distorted for other values of p. However, as the SNR decreases to 10 dB, the p must be equal to 28 or 32 in order to achieve the same 0.5 MHz spectral resolution. The recommended $p = 2 N / 3$ from [4] cannot provide 0.5 MHz spectral resolution for

83

SNR equals to 10 dB. Though processing time is relatively low, the actual time for spectrum estimation needs to factor in the time to estimate the number of frequencies, M, in the received signal.

For ESPRIT, the smallest spectral resolution achievable is 0.1 MHz, which is better than that of the MUSIC at 0.5 MHz. The maximum estimation error is small and comparable to that of MUSIC. The accuracy of the power spectrum is more dependent on the accuracy of the estimated number of frequencies, M, in the received signal. If M is over-estimated, (M - 6) frequencies will be falsely detected. If M is under-estimated, (6 - M) frequencies in the received signal will not be detected. For SNR smaller than 30 dB, the ESPRIT's spectral resolution drops from 0.1 MHz to 0.5 MHz. This shows that the spectral resolution of the ESPRIT is not robust to the presence of noise. As the SNR decreases from 30 dB to 10 dB, the maximum estimation error increases significantly from 0.042 MHz to 1.061 MHz. At 10 dB, the ESPRIT under-performs the MUSIC. Both methods can provide 0.5 MHz spectral resolution, but the ESPRIT has a higher maximum estimation error of 1.061 MHz, as compared to that of the MUSIC at 0.1 MHz. Similar to the MUSIC, the actual time for spectrum estimation needs to factor in the time to estimate the number of frequencies, M, in the received signal. However, it should be noted that the MATLAB processing time is typically much longer than that for a compiled program, such as LABVIEW.

Table 6.   Summary of Simulation Results.

Method	SNR (dB)	Resolution (MHz)	Input Parameters	Max. Error (MHz)	Max. Processing Time (s)	Remarks
MUSIC ($T_w = 1$ μs)	Noiseless	0.5	$M = 7$ $p = 16$	0.1	0.112968	-20 MHz not detected
		0.5	$M = 7$ $p = 20, 24, 28,…, 92$	0.1	0.132163	Spectrum is distorted except for the stated values of p
	10	1	$M = 7$ $p = 24, 36, 40,…,92$	0.2	0.119846	
		0.5	$M = 7$ $p = 28, 32$	0.1	0.092939	
ESPRIT ($T_w = 1$ μs)	Noiseless	0.1	$M = 6$	0.216	0.013297	If $M > 6$, (M - 6) false detections. If $M < 6$, (6 - M) fail detections.
	10	0.5		1.061	0.013671	
	15	0.5		0.041	0.013439	
	20	0.5		0.043	0.014302	
	25	0.5		0.038	0.014107	
	30	0.5		0.042	0.012422	
MRSS	Noiseless	1	$T_w = 3$ μs	0	1.568335	f_{sweep} = 10 kHz
		0.5	$T_w = 5$ μs	0	1.715302	
		0.1	$T_w = 9$ μs	0	2.396204	
	10	1	$T_w = 3$ μs	0	1.670444	
		0.5	$T_w = 5$ μs	0	1.694698	
		0.1	$T_w = 9$ μs	0	2.020169	
	0	1	$T_w = 3$ μs	0	1.615260	
		0.5	$T_w = 5$ μs	0	1.752301	
		0.1	$T_w = 9$ μs	0	1.986819	
	-10	1	$T_w = 3$ μs	0	1.527710	
		0.5	$T_w = 5$ μs	0	1.642263	
		0.1	$T_w = 13$ μs	0	2.184246	

Unlike the MUSIC and ESPRIT, MRSS does not require prior estimation of the number of frequencies, M, in the received signal, nor input of the order of the filter, p. The MRSS needs at least 3 μs of observation time, T_w, in order to produce a stable spectrum of 1 MHz resolution. The value of T_w has to be increased to 5 μs, so as to

increase the frequency resolution to 0.5 MHz. To achieve 0.1 MHz spectral resolution, the value of T_w has to be further increased to 9 μs. With thrice the value of T_w, the MRSS out-performs the MUSIC and ESPRIT at SNR equals to 10 dB and zero maximum estimation error. The processing time of the MRSS is about 124 times more than that of the ESPRIT. However, the required observation time, T_w, remains relatively small at 2.4 μs. The MRSS is exceptionally robust to the presence of noise in the received signal. When the SNR is lowered to 0 dB for T_w equals to 9 μs, the MRSS is able to preserve its spectral resolution at 0.1 MHz and maximum estimation error at zero. When the SNR is furthered lowered to -10 dB, the observation time, T_w, is only required to be lengthened by another 4 μs to 13 μs for the MRSS to retain its 0.1 MHz spectral resolution and zero maximum estimation error.

C.   CONCLUSION

The MRSS out-performs the MUSIC and ESPRIT in terms of spectral resolution, estimation accuracy, and robustness to noise. Though the MRSS requires a higher observation time and processing time, the values remain significantly low at 13 μs and 2.4 μs respectively for SNR equals to -10 dB. These values meet the requirements of a digital array system. Hence, this thesis proposes the use of the MRSS algorithm in the frequency estimation module in the digital tracking array to provide accurate, robust, and high resolution spectrum estimation.

An advantage of the digital architecture is that multiple frequency estimation processors can be loaded and the specific one selected based on the available data (SNR, observation time, etc.).

D.   FUTURE WORKS

For a digital tracking array, a small observation time is required to provide fast response. In this thesis, AWGN noise is generated and added to the simulated received signal over this short observation window. The performances of the high resolution spectrum estimation methods are measured and evaluated. However, due to the randomness of the noise and the short observation time, the specific values of the order of

the filter, p, of the MUSIC and ESPRIT might vary slightly. Similarly, the observation time, T_w, required of the MRSS might vary slightly with respect to the SNR. To determine the design parameter of p or T_w, statistical modeling using Monte Carlo simulations is recommended.

THIS PAGE INTENTIONALLY LEFT BLANK

LIST OF REFERENCES

[1]   B. L. Gezer, "Multi-beam Digital Antenna for Radar, Communications, and UAV Tracking Based on Off-the-Shelf Wireless Technologies," Master's Thesis, Naval Postgraduate School, Monterey, California, December 2006.

[2]   Anthony Lee, "Variable Resolution Direction Finding using the Robust Symmetrical Number System," Master's Thesis, Naval Postgraduate School, Monterey, California, December 2006.

[3]   Kevin Kwai, "An Analysis of Three-Channel RSNS Virtual Spacing Direction Finding System," Master's Thesis, Naval Postgraduate School, Monterey, California, December 2007.

[4]   James B. Tsui, *Digital Techniques for Wideband Receivers*, pp. 111–113, pp. 449–508, 2nd edition, SciTech, 2004.

[5]   National Instruments, "Zero Padding Does Not Buy Spectral Resolution," September 6, 2006, http://zone.ni.com/devzone/cda/tut/p/id/4880, accessed September 8, 2009.

[6]   MATLAB Help File, MATLAB version 7.5.0.342 (R2007b), August 15, 2007.

[7]   Y. Hur, J. Park, W. Woo, K. Lim, C.-H. Lee, HS. Kim, and J. Laskar, "A wideband analog multi-resolution spectrum sensing (MRSS) technique for cognitive radio (CR) systems," *Proc. of IEEE International Symposium on Circuits and Systems*, pp. 4090–4093, 2006.

THIS PAGE INTENTIONALLY LEFT BLANK

INITIAL DISTRIBUTION LIST

1.   Defense Technical Information Center
        Ft. Belvoir, Virginia

2.   Dudley Knox Library
        Naval Postgraduate School
        Monterey, California

3.   Chairman, Code EC
        Naval Postgraduate School
        Monterey, California

4.   Professor David C. Jenn
        Department of Electrical & Computer Engineering
        Naval Postgraduate School
        Monterey, California

5.   Professor Phillip E. Pace
        Department of Electrical & Computer Engineering
        Naval Postgraduate School
        Monterey, California

6.   Professor Kevin D. Jones
        Department of Mechanical & Astronautical Engineering Department
        Naval Postgraduate School
        Monterey, California

7.   Professor Yeo Tat Soon
        Temasek Defence Science Institute
        National University of Singapore
        Singapore

8.   Tan Lai Poh (Ms)
        Temasek Defence Science Institute
        National University of Singapore
        Singapore

9.   Yeo Kwang Hui
        Singapore Army
        Singapore

10.   Tan I-Hsiang
        ST Electronics
        Singapore